1998

Analysis of Taper-Taper Adhesive-Bonded Joints in Composite Plates Under Tension and Cylindrical Bending.

Jack Elwin Helms Jr
Louisiana State University and Agricultural & Mechanical College

INFORMATION TO USERS

This manuscript has been reproduced from the microfilm master. UMI films the text directly from the original or copy submitted. Thus, some thesis and dissertation copies are in typewriter face, while others may be from any type of computer printer.

The quality of this reproduction is dependent upon the quality of the copy submitted. Broken or indistinct print, colored or poor quality illustrations and photographs, print bleedthrough, substandard margins, and improper alignment can adversely affect reproduction.

In the unlikely event that the author did not send UMI a complete manuscript and there are missing pages, these will be noted. Also, if unauthorized copyright material had to be removed, a note will indicate the deletion.

Oversize materials (e.g., maps, drawings, charts) are reproduced by sectioning the original, beginning at the upper left-hand corner and continuing from left to right in equal sections with small overlaps. Each original is also photographed in one exposure and is included in reduced form at the back of the book.

Photographs included in the original manuscript have been reproduced xerographically in this copy. Higher quality 6" x 9" black and white photographic prints are available for any photographs or illustrations appearing in this copy for an additional charge. Contact UMI directly to order.

UMI

A Bell & Howell Information Company
300 North Zeeb Road, Ann Arbor MI 48106-1346 USA
313/761-4700 800/521-0600

ANALYSIS OF TAPER-TAPER ADHESIVE-BONDED JOINTS IN COMPOSITE PLATES UNDER TENSION AND CYLINDRICAL BENDING

A Dissertation

Submitted to the Graduate Faculty of the
Louisiana State University and
Agricultural and Mechanical College
in partial fulfillment of the
requirements for the degree of
Doctor of Philosophy
in

The Department of Mechanical Engineering

by
Jack E. Helms, Jr.
B.S., Henderson State College, 1970
B.S., University of Arkansas, 1974
M.S., University of Arkansas, 1975
May 1998

DEDICATION

This dissertation is dedicated to my wife Mary who willingly took on many new duties so that I could study and work on my research. Her love, support, sacrifices, and encouragement sustained me through the difficult times when the work was hard and seemingly endless. I could not have done this without her by my side.

And also to my children, Daniel and Emily. They sacrificed many hours of time with me to allow me to pursue this degree. Their encouragement helped me through each day.

ACKNOWLEDGMENTS

This dissertation was partially sponsored by fellowship grants from the American Welding Society as well as the Louisiana Board of Regents under contract numbers LEQSF (1994-97)-RD-B-02, LEQSF (1995-98)-RD-B-05, and LEQSF (1996-99)-ENH-PLEx-03.

The author wishes to thank his major advisor, Dr. Su-Seng Pang without whose help this dissertation would not have been possible. Dr. Chihdar Yang, now of Wichita State University, served as co-advisor, mentor, and friend. My Advisory Committee also consisted of Dr. Aravamudhan Raman and Dr. Medhy Sabbaghian of Mechanical Engineering, Dr. George Z. Voyiadjis of Civil Engineering (minor advisor), Dr. John R. Collier of Chemical Engineering, and Dr. William A. Adkins of the Mathematics Department. Their time, comments and suggestions were greatly appreciated.

Several fellow graduate students contributed to my program of study as classmates, friends and encouragers: Dr. Michael A. Stubblefield, now of Southern University, Karen E. Crosby, H. Dwayne Jerro, Patrick F. Mensah, and Yi Zhao. They were always around to discuss classwork and research, offer help and suggestions, and sometimes to just talk.

Several supervisors of the Albemarle Corporation made my program possible by granting me time off to attend classes and conferences. Their understanding and support were essential to my completion of this degree.

TABLE OF CONTENTS

LIST OF TABLES

LIST OF FIGURES

ABSTRACT

A taper-taper adhesive-bonded joint between two composite plates has been analyzed under tension and cylindrical bending.

Two tension models were derived. The first model was based on mechanics of materials and the second model used laminated plate theory and shear correction factors. For the mechanics of materials model the condition of plane strain was assumed for the adherends and adhesive. Average stresses were used in the adherends and point-wise stresses were used in the adhesive. The model derived consisted of four second-order ordinary differential equations with variable coefficients. The adherends were characterized by the extensional Young's modulus. The equations were solved numerically using the Linear Shooting Method and the solutions were compared with finite element models developed using the COSMOS/M commercial software package. The model was accurate in the area away from the sharp end of the taper and predicted strains within about 5-10% of the finite element models. The second analytical model was developed to improve prediction near the sharp end of the taper. The model was derived using first-order, laminated plate theory and included transverse shear deformation effects. The assembly was divided into three areas to facilitate the analysis, the two sections of laminate away from the joint and the joint itself. The first two sections were modeled by three first-order differential equations each. The joint was modeled by six second-order, ordinary differential equations with variable coefficients. The six equations were reduced to a set of twelve first-order differential equations, which were solved numerically with the six first-order equations from

the areas away from the joint. Finite element models were developed using the COSMOS/M commercial software package for verification of the model. The model was accurate and predicted the peak stresses within about 5-8 % of the values calculated with finite element analysis.

A laminated plate model of the taper-taper joint was also derived for the case of cylindrical bending. The FORTRAN program was modified to numerically solve the resulting system of twelve first-order differential equations with variable coefficients. The adhesive stresses predicted were within about 2% of the results from the finite element models.

CHAPTER 1

INTRODUCTION

Fiber-reinforced polymer composite materials are used in the chemical process industries because of their light weight, high strength-to-weight ratio, directional properties and high corrosion resistance. The fibers are used to carry the loads and the matrix is used to fix the shape of the component. Modern composites incorporate high performance fibers such as carbon, boron, and Kevlar as well as glass. New matrix materials are also routinely developed. One of the primary advantages available with composites is the ability to tailor the stiffness in a particular direction by varying the laminate stacking sequence.

Joints are normally the weakest part of a structure but some are required in almost all real applications. In many applications adhesive-bonded joints have replaced bolted joints because of the laminate damage inherent to the drilling process, the stress concentration developed due to the holes, the weight penalty of the bolting, and susceptibility of the bolting material to corrosion. Joint design in industry is largely based on engineering judgement tempered with experience or experimental studies. The lack of easily used analytical design methods prevents adhesive-bonded joints from being used to their full potential. These factors highlight the need for additional research in the field of adhesive-bonded joint design and analysis.

Finite element methods can be used to solve many design and analysis problems with different materials and geometries. However, analytical solutions are still desired for further analyses such as optimization of joint geometry.

This present research was initiated because of an industrial design problem that was encountered several years ago. A joint design was developed to reduce the cost of a 14 to 18 inch composite piping system. The system was initially designed with standard couplings and an overlay at each end of the coupling to ensure the integrity of the buried pipeline. The high estimated cost of each joint, due to the coupling, two overlays and the associated labor, led to the consideration of a more economical joint design. The design team developed a taper-taper joint with a single overlay. The taper angle was chosen based on difficulty of machining and assembly and engineering judgment. The piping system has been in service for several years without any problems and it must be concluded that the design was conservative. However, since there were several miles of piping involved the question of efficiency and cost of the joint is still of interest. The initial effort in this study involved a mechanics of materials model of the taper-taper pipe joint. The results achieved were not entirely adequate and further research was undertaken to gain an understanding of the taper-taper joint between flat plates.

1.1 Work to be Done

Previous analyses of the taper-taper joints have been limited to small and large angle ranges, and in some cases one or both of the adherends have been isotropic. This was done to model actual structures and in some cases to simplify the analyses mathematically and make the research manageable. If this joint is to reach its full potential for use, better analytical design tools must be developed. In this research models are developed for taper-taper joints where both adherends are unidirectional or crossply laminates. The angles chosen for modeling are in the intermediate range. Models are developed for tension

loading. A second laminated plate model is derived and solved for the case of cylindrical bending.

1.2 Scope, Goals, and Objectives

The scope of this research was to develop analytical models of the adhesive-bonded taper-taper joint between two laminates under tension and cylindrical bending.

The specific goals were to derive two analytical models for an adhesive-bonded taper-taper joint between two anisotropic laminated plates under tension loading. Laminated plate theory was also to be used to derive a model for the case of cylindrical bending.

The objective of the research was to derive a mechanics of materials model and a laminated plate model for tension loading. A laminated plate model was also to be derived for cylindrical bending. All three models were to be solved numerically. FORTRAN computer programs were to be developed to integrate the systems of simultaneous differential equations of the three models. These programs were necessarily specific to the different laminates chosen for study, but could be generalized to other laminates combinations by modifying one subroutine to reflect different materials, different number of ply groups, and different lay-up sequences.

A preliminary buckling analysis of the taper-taper joint was also carried out using laminated plate theory. The derivation of the model and the resulting stiffness matrix elements are presented in Appendices A and B.

CHAPTER 2

PREVIOUS WORK

2.1 General

There is a growing body of literature covering adhesive-bonded joints in composites that spans about the last fifty years. The early analytical work on isotropic adherends prior to 1961 was reviewed by Kutscha [1], and the analyses from 1961 to 1969 were reviewed by Kutscha and Hofer [2]. Matthews, *et al.* [3] reviewed the classical and finite element analyses related to all aspects of adhesive-bonded joints in composite materials. Vinson [4] produced a summary of the published work concerning the adhesive bonding of polymer matrix composite structures in 1989. Hart-Smith [5] published a paper covering the analysis and design of advanced composite bonded joints. Adams and Wake [6] published a book covering structural adhesive joints. Adams and Wake noted that one of the benefits of using adhesive-bonded joints was that the resulting stress distribution was more uniform than for bolted joints. They also noted that non-linearities can be caused by joint rotation and material plasticity and warned that large stress gradients, approaching singularities, are possible in adhesive-bonded joints. Therefore finite element models must use a sufficient number of elements of the appropriate complexity in areas where the gradients may exist.

Many researchers have developed new or refined theories for describing the behavior of plates. Baluch, *et al.* [7] developed a new theory for isotropic plates that included transverse shear, normal stress and normal strain. Voyiadjis, *et al.* [8] extended plate theory to account for the effects of transverse normal strain in bending of isotropic plates. Several papers have been published noting the importance of including transverse shear effects in

the analysis of composite plates when the span-to-depth ratio is small [9]-[12] and noted that these effects can significantly affect gross plate response for anisotropic plates. Khedir, *et al.* [13] made refinements to shear deformation theory and calculated a Levy type solution for symmetric laminated composite plates. Whitney and Leissa [14] extended thin-plate theory by including non-linear terms and rotary inertia. Closed forms solutions were calculated for the linearized form of their model. Lo, *et al.* [15], [16] included the effects of transverse shear deformation, transverse normal strain and a non-linear distribution of the in-plane displacements. Medwadowski [17] developed a theory for classic, orthotropic plates with large deflections. He included transverse shear deformation and normal stress. Levy type solutions were calculated for the linearized form of the equations.

Whitney [18] conducted an analysis of bending-extensional coupling in antisymmetric cross-ply and angle-ply laminates under transverse loading. Classical small deflection, thin plate theory was used and closed form solutions were derived using Fourier Series techniques. Whitney concluded that coupling can increase deflection by as much as 300%. The real effect of bending-extensional coupling is reduction of the plate stiffness.

Pagano [19] compared classical laminated plate theory (CPT) to theory of elasticity solutions under cylindrical bending. He concluded that classical plate theory leads to a very poor description of laminate response at low span-to-depth ratios, but converges to the exact solution as the ratio increases. Whitney [20] studied the cylindrical bending of unsymmetrically laminated plates. Cylindrical bending provides a useful approximation of the behavior of rectangular laminated plates having a high length-to-width ratio. Pagano [21] investigated static bending of composite plates by considering shear coupling. The

exact solutions calculated approach classical plate theory as the span-to-depth ratio increases.

A number of researchers have developed higher-order theories in an attempt to more accurately describe the behavior of plates under loads. Toledano and Murakami [22] developed a higher-order laminated plate theory based on Reissner's mixed variational principle. The theory accurately estimated in-plane responses even for small span-to-thickness ratios. Pandya and Kant [23] derived a simple isoparametric finite element formulation based on higher-order displacements for flexure analysis of multilayer symmetric sandwich plates. Reddy [24] published a higher order shear deformation theory that was based on a parabolic distribution of transverse shear strains. Closed form solutions were obtained for symmetric cross-ply laminates.

Many of the analyses in the literature neglect edge effects. Spilker and Chou [25] developed a special-purpose hybrid-stress multilayer finite element formulation that satisfies the traction-free-edge condition exactly.

Pagano [26] calculated three dimensional elasticity solutions for rectangular bidirectional composite and sandwich plates. His approach is sufficiently general to describe the exact elastic response of rectangular, pinned edge laminates consisting of any number of orthrotropic or isotropic layers. Pipes and Pagano [27] studied interlaminar stresses under axial extension. Interlaminar shear stress was found to be an edge effect which is localized in the edge region that is approximately as wide as the laminate thickness.

Chou and Carleone [28] extended Mindlin's theory to laminated plates by considering transverse shear. The theory produces good results without shear correction

factors. Whitney [29] extended the procedure of Chow to orthrotropic laminates of non-symmetric construction and compared the results to exact elasticity solutions.

2.2 Lap Joints

Goland and Reissner [30] analyzed a single lap joint with isotropic adherends and adhesive. This analysis was the first to include the effects of rotation of the adherends. They related the bending moment to the in-plane loading at the end of the overlay. Hart-Smith [31], [32] published papers covering single-lap and double-lap joints using a continuum model in which the adherends were isotropic or anisotropic elastic, and the adhesive was modeled as elastic, elastic-plastic, or bielastic. Hart-Smith used plate theory as the starting point in his derivations. The effects of transverse shear deformation have been shown to be important when the span-to-depth ratio is small or when the transverse shear modulus is small [33], [34]. However, these effects were not included in Goland and Reissner or Hart-Smith's theories. Edge effects have been neglected and adhesive stresses assumed constant through the thickness in most of the analyses found in the literature. Sharpe and Muha [35] conducted experimental studies of a lap joint using plexiglass models and a laser fringe technique. McLaren and MacInnes [36] used photoelasticity techniques to study the stress distribution of a lap joint. Wah [37] conducted a theoretical analysis of a single lap joint using the theory of elasticity. Allred and Guess [38] studied double lap joints under bending using finite elements and experimental techniques. Cheng, *et al.* [39] provided a two dimensional elasticity solution of lap joints with adherends of different thickness, lengths and materials. Delale, *et al.* [40] conducted an analytical stress analysis of a single lap joint constructed of different isotropic adherends. Renton [41] analyzed a the

symmetric lap shear test and developed a closed form solution. The solution was verified experimentally using optical and photoelastic methods. Griffin, *et al.* [42] analyzed an adhesive-bonded composite pipe joint and derived a mathematical model of the stress-strain behavior of the joints. Yang and Pang [43] analyzed the stress-strain distribution in a single lap-joint under tension loading. The analysis included transverse shear deformation effects and closed form solutions were achieved. The solutions were verified using finite element analysis.

2.3 Stepped and Tapered Joints

The terms scarf and bevel joint are used for more than one type of joint in the literature and therefore the term taper-taper was adopted for the type of joint analyzed in this research. Hart-Smith [44] also analyzed taper-taper and stepped-lap joints using the same type of analysis he used for single and double lap joints. The taper-taper joint has higher efficiency than the lap joint and the efficiency of a stepped lap lies somewhere in between. The shear stresses in a taper-taper joint are very uniform if identical adherends are used. Hart-Smith stated that it is common design practice with small taper angles to neglect adhesive tension or compression stresses. Small angles were defined as angles less than 4°. Adhesive peel stresses were therefore omitted by Hart-Smith in his research. Wah [45] analyzed a taper-taper joint of arbitrary angle under pure bending. The approach used was classical two dimensional elasticity assuming elastic, isotropic adherends and adhesive. The adhesive was also considered to be a thin film. The model was derived under the condition of plane stress. Sage [46] analyzed a taper-taper joint between alloy and a carbon fiber composite adherends. He performed fatigue tests under pure shear loading. The fatigue

strength was well below that of the adhesive in pure shear. Erdogan and Ratwani [47] derived models for the strains and stresses in stepped-lap and taper-taper joints under the assumption of generalized plane stress. The taper-taper joint was considered as the limit of a stepped joint, i.e., a joint with an infinite number of steps. The stepped joint approximation provides a good check on the analytical models developed in this research because a closed form solution was obtained. Figure 1 shows the dimensions and layout of the stepped joint.

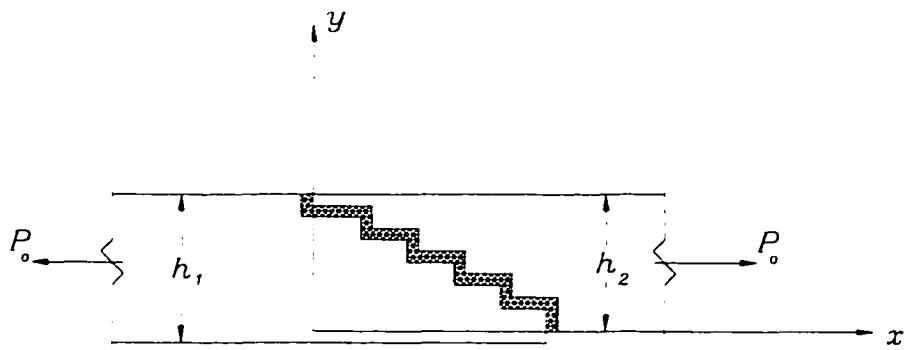

Figure 1 Adhesive Bonded Stepped Joint

A second order ordinary differential equation is derived for the force per unit width, p_{2i}. The equation is

$$\frac{d^2 p_{2i}}{dx^2} - \alpha_i^2 p_{2i} = \beta_i p_o \quad (i = 1,\ldots,n) \tag{1}$$

where n is the number of steps, p_o is the applied load per unit width and

$$\alpha_i^2 = \frac{G_3}{h_3}\left[\frac{1-\nu_1^2}{E_1 h_{1i}} + \frac{1-\nu_{2x}\nu_{2z}}{E_{2x} h_{2i}}\right]$$
$$\beta_i = -\frac{G_3}{h_3}\frac{1-\nu_1^2}{E_1 h_{1i}} \tag{2}$$

where ν_1 is Poisson's ratio for the isotropic left plate, ν_{2x} and ν_{2z} are the Poisson's ratios for the right plate. E_1 is Young's modulus for the left plate, E_{2x} is Young's modulus of the right plate in the x direction, and G_3 is the shear modulus of the adhesive. h_{1i} and h_{2i} are the thicknesses of the laminate at the step under consideration and h_3 is the adhesive thickness. The solution of Eq. 1 may be written as

$$p_{2l}(x) = A_l e^{-\alpha_l x} + B_l e^{\alpha_l x} - \frac{\beta_l p_o}{\alpha_l^2} \quad (l = 1,\ldots,n) \tag{3}$$

The 2n integration constants are determined by assuming continuity of forces and their derivatives at the end of each step. Strains and stresses can then be calculated from the forces and material properties. Helms, *et al.* [48] developed a mechanics of materials model of a taper-taper adhesive-bonded joint between two composite flat plates that accurately predicted strains in the joint away from the sharp end of the taper.

The models discussed above do not adequately describe the taper-taper joint. Hart-Smith [44] modeled only small taper angles, neglected peel stresses and did not include transverse shear deformation. Wah [45] modeled arbitrary angles, but only included isotropic adherends and did not include transverse shear deformation. Sage [46] investigated only fatigue under pure shear. Erdogan and Ratwani [47] did not include transverse shear deformation and used the extensional modului to characterize the adherends. Helms, *et al.* [49] developed a model that incorporated the equivalent modulus matrices, included transverse shear deformation effects and modeled arbitrary angles. The laminated plate model developed in this research extends the state of the art of analysis of

the taper-taper joint. The numerical solution of the model was verified using finite element models.

CHAPTER 3

TENSION LOADING

3.1 Mechanics of Materials Model

A mathematical model of the joint has been developed under the following assumptions: 1) the adherends are under the condition of plane stress; 2) the plate and adhesive are assumed to be linear elastic materials; 3) the adhesive was assumed to be isotropic and the extensional Young's modulus of the plate was used to characterize the adherends; 4) average stresses were used within the plate to simplify the derivation; 5) the adhesive was the weakest part of the joint and would fail by peeling or shearing before either of the plates failed; and 6) the adhesive layer has a constant thickness throughout the joint. Use of the average stresses within the plate was acceptable because the adhesive was assumed to have been weaker than the composite plates. The average stresses were assumed constant across each cross section cut perpendicular to the x axis.

Figure 2 is a pictorial representation of the joint. Figure 3 is a freebody diagram of the joint that was used to facilitate the derivation of the equations. The equations are written in terms of average stresses within the plate and point-wise stresses within the adhesive. Since average stresses are used in modeling the plate, the stresses are considered to be functions of the distance along the plate only. There is no external applied moment because the tension load is applied along the long (x) axis of the plates and through the geometric center. Therefore there will be no rotation of the plates due to the applied loading. The moment equations were not included since they would only show the location of the point of application of the equivalent force on the cross section.

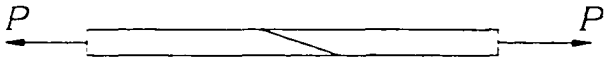

Figure 2 Pictorial View of the Joint - Mechanics of Materials Model

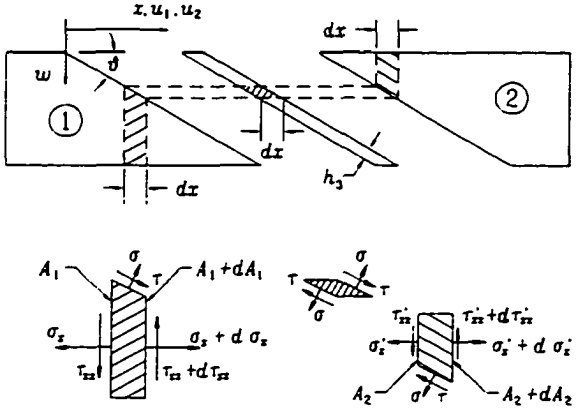

Figure 3 Freebody Diagram of the Joint - Mechanics of Materials Model

A force balance yields the following equations in terms of the stresses:

$$(\sigma_x + d\sigma_x)(A_1 + dA_1) - \sigma_x A_1 + (\sigma \sin\theta + \tau \cos\theta) A_s = 0 \qquad \textbf{(4)}$$

$$(\tau_{xz} + d\tau_{xz})(A_1 + dA_1) - \tau_{xz} A_1 + (\sigma \cos\theta - \tau \sin\theta) A_s = 0 \qquad \textbf{(5)}$$

$$(\sigma'_x + d\sigma'_x)(A_2 + dA_2) - \sigma'_x A_2 - (\sigma \sin\theta + \tau \cos\theta) A_s = 0 \qquad \textbf{(6)}$$

$$(\tau'_{xz} + d\tau'_{xz})(A_2 + dA_2) - \tau'_{xz} A_2 - (\sigma \cos\theta - \tau \sin\theta) A_s = 0 \qquad \textbf{(7)}$$

where A_1 and A_2 are the cross-sectional areas for a unit width of the plates, and A_s is the shear area for a unit width of the joint. σ_x and τ_{xz} are the normal and shear stresses in the left-hand plate and the primed stresses are for the right-hand plate. σ and τ are the normal and shear stresses in the adhesive. Multiplying out the terms in the equations above,

eliminating second order differentials, and dividing by dx yields the following:

$$A_1 \frac{d\sigma_x}{dx} + \sigma_x \frac{dA_1}{dx} + (\sigma \sin\theta + \tau \cos\theta) \frac{A_s}{dx} = 0 \quad \textbf{(8)}$$

$$A_1 \frac{d\tau_{xz}}{dx} + \tau_{xz} \frac{dA_1}{dx} + (\sigma \cos\theta - \tau \sin\theta) \frac{A_s}{dx} = 0 \quad \textbf{(9)}$$

$$A_2 \frac{d\sigma_x'}{dx} + \sigma_x' \frac{dA_2}{dx} - (\sigma \sin\theta + \tau \cos\theta) \frac{A_s}{dx} = 0 \quad \textbf{(10)}$$

$$A_2 \frac{d\tau_{xz}'}{dx} + \tau_{xz}' \frac{dA_2}{dx} - (\sigma \cos\theta - \tau \sin\theta) \frac{A_s}{dx} = 0 \quad \textbf{(11)}$$

where the areas for a strip of unit width can be expressed as:

$$A_1 = h - x \tan\theta \quad \textbf{(12)}$$

$$A_2 = x \tan\theta \quad \textbf{(14)}$$

$$A_s = \frac{dx}{\cos\theta} \quad \textbf{(13)}$$

where h is the plate thickness, θ is the taper angle, A_1 and A_2 are the areas for the left and right plate, and A_s is the shear area of the adhesive. In general, adhesives often act as bilinear or elastic plastic solids. However, in this model the applied loading is far from that which would cause failure of the joint. For this reason the adhesive can be modeled as an elastic solid. And the equations used by Erdogan and Ratwani, which modeled the adhesive as tension and shear springs [47] were chosen:

$$\sigma = \frac{E_3}{h_3}\left[(u_2 - u_1)\sin\theta - (w_2 - w_1)\cos\theta\right] \tag{15}$$

$$\tau = \frac{G_3}{h_3}\left[(u_2 - u_1)\cos\theta + (w_2 - w_1)\sin\theta\right] \tag{16}$$

where G_3, E_3, and h_3 are the shear modulus (GPa), elastic modulus (GPa), and thickness (mm) of the adhesive, respectively, and E and G are the extensional Young's modulus (GPa) and shear modulus (GPa) of the plates. u_1 and u_2 are the displacements along the left and right plates in mm and w_1 and w_2 are the vertical displacements of the left and right plates in mm. θ is the taper angle in degrees. The stresses can be related to the displacements through the use of Hooke's Law:

$$\sigma_x = E\frac{du}{dx} \quad ; \quad \tau_{xz} = G\left(\frac{dw}{dx} + \frac{du}{dz}\right) \tag{17}$$

Since the integrated average stresses are used, $du/dz = 0$. Substituting Eqs. (12 - 17) into Eqs. (8 - 11) yields:

$$\begin{aligned} & E\,(h - x\tan\theta)\frac{d^2u_1}{dx^2} - E\tan\theta\frac{du_1}{dx} \\ & + \frac{E_3}{h_3}\left[(u_2 - u_1)\sin\theta\tan\theta + (w_2 - w_1)\sin\theta\right] \\ & + \frac{G_3}{h_3}\left[(u_2 - u_1)\cos\theta + (w_2 - w_1)\sin\theta\tan\theta\right] = 0 \end{aligned} \tag{18}$$

$$G\,(h - x\tan\theta)\,\frac{d^2w_1}{dx^2} - G\tan\theta\,\frac{dw_1}{dx} + \frac{E_3}{h_3}\,[(u_2 - u_1)\sin\theta + (w_2 - w_1)\cos\theta] - \frac{G_3}{h_3}[(u_2 - u_1)\cos\theta + (w_2 - w_1)\sin\theta\tan\theta] = 0 \tag{19}$$

$$E\,(x\tan\theta)\,\frac{d^2u_2}{dx^2} + E\tan\theta\,\frac{du_2}{dx} - \frac{E_3}{h_3}\,[(u_2 - u_1)\sin\theta\tan\theta + (w_2 - w_1)\sin\theta] - \frac{G_3}{h_3}\,[(u_2 - u_1)\cos\theta + (w_2 - w_1)\sin\theta\tan\theta] = 0 \tag{20}$$

$$G\,(x\tan\theta)\,\frac{d^2w_2}{dx^2} + G\tan\theta\,\frac{dw_2}{dx} - \frac{E_3}{h_3}[(u_2 - u_1)\sin\theta + (w_2 - w_1)\cos\theta] + \frac{G_3}{h_3}\,[(u_2 - u_1)\sin\theta + (w_2 - w_1)\sin\theta\tan\theta] = 0 \tag{21}$$

These equations are linear, coupled, second order differential equations with variable coefficients. The equations must be solved numerically subject to the boundary conditions below. For both plates it is assumed that the stress is uniformly distributed in the regions away from the taper-taper joint, and that the stress is zero on the free surface on the end of the truncation. It is assumed that the shear stress develops due to the taper and is essentially zero away from the joint.

For the left plate:

$$\frac{du_1}{dx}\Big|_{x=0} = \frac{P}{E\,h}\ ; \qquad \frac{du_1}{dx}\Big|_{x=L} = 0 \tag{22}$$

$$\frac{dw_1}{dx}\Big|_{x=L} = 0 \tag{23}$$

For the right plate:

$$\frac{du_2}{dx}\Big|_{x=0} = 0\ ; \qquad \frac{du_2}{dx}\Big|_{x=L} = \frac{P}{E\,h} \tag{24}$$

$$\frac{dw_2}{dx}\Big|_{x=0} = 0 \tag{25}$$

The four second-order equations were reduced to a set of eight first-order equations by an order reduction method [60]. An algorithm based on the Linear Shooting Method [61] was developed to solve this boundary value problem. Solution of the eight equations required two additional boundary conditions. The deflections at the left end of the joint were assumed to be:

$$w_1|_{x=0} = 0 \tag{26}$$

$$u_1|_{x=0} = 0 \tag{27}$$

The Shooting Method converts boundary-value problems to initial-value problems. The equations are integrated from left to right and the values of the variables calculated are compared to known boundary values at the right end of the joint. The assumed initial values

are then adjusted and the equations are integrated again. The process is continued until the differences between the calculated values and the known boundary conditions are reduced to a small quantity. A computer program was written in FORTRAN to implement the algorithm on an IBM compatible personal computer. The program calculated strains along the plate where strains were assumed to be constant across a cross-section. The program was run for taper angles of 20° and 25° for 6.35 mm plate and at taper angles of 15° and 20° for 3.175 mm plate.

3.2 Laminated Plate Model

The mechanics of materials model uses the extensional Young's modulus to characterize the behavior of the adherends. This approach is adequate for gross extensional behavior of the non-tapered portion of the adherends. However, in the tapered portions of the adherends this method does not accurately represent the change in stiffness from laminae to laminae, but approximates it linearly. Use of the equivalent modulus matrices will more accurately represent the fractional stiffness that results from removing material to form the taper. Classical first order laminated plate theory is used in the derivations that follows. Transverse shear deformation effects are included through the use of shear correction factors. The tension and shear spring model of the adhesive used in the first model was replaced by a model based on derivatives of the strains.

The main advantage of the laminated plate model is that pointwise strains and stresses can be calculated since the change in laminate properties from ply group to ply group are more accurately represented. This advantage is offset by the increased mathematical difficulty of the model and the additional computational effort involved in

integrating the eighteen differential equations versus the eight differential equations of the first analytical model.

Figure 4 shows the configuration of the taper-taper joint under tension. The tensile loading, shown as P, represents a loading per unit width.

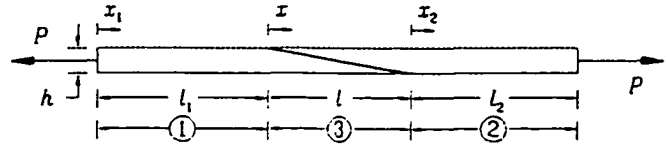

Figure 4 Tension Loading - Laminated Plate Model

Figure 5 shows the coordinate system of the joint

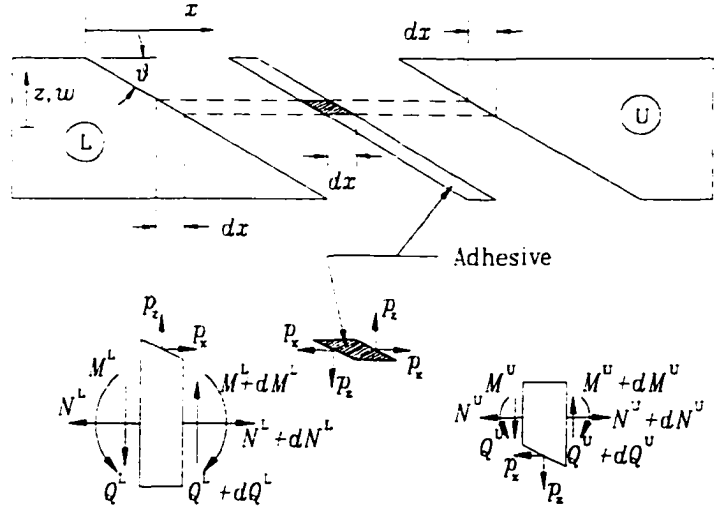

Figure 5 Freebody Diagram of the Joint - Laminated Plate Model

Based on first-order, laminated plate theory, the displacement field of the two laminates in the x and z-directions can be written as

$$u=u^{o}(x)+z\psi(x) \tag{28}$$

$$w=w(x) \tag{29}$$

where the superscript u^o represents the mid-plane displacement, ψ is its corresponding bending slope, and x is a general length variable and applies to all sections of the joint. By substituting Eqs. (28) and (29) into the strain-displacement relations, the normal strain ϵ_x and shear strain ϵ_{xz} can be expressed as

$$\epsilon_x = \epsilon_x^o + z\frac{d\psi}{dx} \tag{30}$$

$$\epsilon_{xz}=\frac{du}{dz}+\frac{dw}{dx}=\psi+\frac{dw}{dx} \tag{31}$$

For laminates constructed of orthotropic laminae, the stress resultant (or unit width force resultant) in the x-direction, N_x, and the unit width moment in the y-direction, M_y , are related to only the mid-plane strain and plate curvature and not to the in-plane shear strain. Because of the assumption of plane strain the stress and moment resultants of the lower and upper laminates are [63]

$$N_x^L = A_{11}^L\frac{du^{oL}}{dx}+B_{11}^L\frac{d\psi^L}{dx} \tag{32}$$

$$N_x^U = A_{11}^U\frac{du^{oU}}{dx}+B_{11}^U\frac{d\psi^U}{dx} \tag{33}$$

$$M_x^L = B_{11}^L \frac{du^{oL}}{dx} + D_{11}^L \frac{d\psi^L}{dx} \tag{34}$$

$$M_x^U = B_{11}^U \frac{du^{oU}}{dx} + D_{11}^U \frac{d\psi^U}{dx} \tag{35}$$

where the $[A]$, $[B]$, $[D]$ are the matrices of the equivalent moduli for the laminate per unit width and the matrices of the equivalent moduli are defined as

$$(A_{11}^L, B_{11}^L, D_{11}^L) = \int_{-h^L/2}^{h^L/2} Q_{11}^{(i)}(1, z_1, z_1^2) dz_1 \tag{36}$$

$$(A_{11}^U, B_{11}^U, D_{11}^U) = \int_{-h^U/2}^{h^U/2} Q_{11}^{(i)}(1, z_2, z_2^2) dz_2 \tag{37}$$

where $Q_{11}^{(i)}$ represent the stiffness in the x-direction of the I th ply. The superscripts L and U denote the lower and upper laminate, respectively, h is the thickness, and z_1 and z_2 are measured from the middle plane of the lower and upper laminates.

From the constitutive relation, the transverse shear stress resultant (or unit width transverse shear force resultant), Q_x can be written as [63]

$$Q_x = kA_{55}\epsilon_{xz} \tag{38}$$

where k is the shear correction factor introduced by Reissner [33] and Mindlin [64]. The A_{55} is defined for the upper and lower laminates as

$$A_{55}^{L} = \int_{-h^{L}/2}^{h^{L}/2} Q_{55}^{(i)} dz_1 \tag{39}$$

$$A_{55}^{U} = \int_{-h^{U}/2}^{h^{U}/2} Q_{55}^{(i)} dz_2 \tag{40}$$

where $Q_{55}^{(i)}$ is the shear stiffness of the i^{th} ply.

The transverse shear stress resultants for the lower and upper laminates can be related to the displacement fields by the substitution of Eq. (31) into Eq. (38).

$$Q_x^{L} = k^{L} A_{55}^{L} (\psi^{L} + \frac{dw^{L}}{dx}) \tag{41}$$

$$Q_x^{U} = k^{U} A_{55}^{U} (\psi^{U} + \frac{dw^{U}}{dx}) \tag{42}$$

The above relations from laminated plate theory correlate the laminate force and moment with the displacement field in terms of the equivalent modulus matrices.

It is convenient to break the joint into three sections as shown in Fig. 4 to facilitate the analysis. The mechanical behavior of the adherends in each section is discussed separately in the following sections.

(a) Section One

Section one is the flat plate to the left of the joint. The axial stress resultant at each section of the lower adherend is

$$N_{x_1}^{L}=P \tag{43}$$

Substituting the kinematic relations into the constitutive relations (Eqs. (32), (34) and (41)), the governing equations of the lower adherend are then

$$\begin{aligned} A_{11}^{L}\frac{du_1^{oL}}{dx_1}+B_{11}^{L}\frac{d\psi_1^{L}}{dx_1}&=P \\ B_{11}^{L}\frac{du_1^{oL}}{dx_1}+D_{11}^{L}\frac{d\psi_1^{L}}{dx_1}+Pw_1^{L}&=0 \\ k^{L}A_{55}^{L}\psi_1^{L}+(k^{L}A_{55}^{L}+P)\frac{dw_1^{L}}{dx_1}&=0 \end{aligned} \tag{44}$$

(b) Section Two

Section two is the flat plate to the right of the joint. The governing equations for the upper laminate are almost the same as those for the lower adherend in section one.

$$\begin{aligned} A_{11}^{U}\frac{du_2^{oU}}{dx_2}+B_{11}^{U}\frac{d\psi_2^{U}}{dx_2}&=P \\ B_{11}^{U}\frac{du^{oU}}{dx_2}+D_{11}^{U}\frac{d\psi_2^{U}}{dx_2}+Pw_2&=0 \\ k^{U}A_{55}^{U}\psi_2^{U}+(k^{U}A_{55}^{U}+P)\frac{dw_2^{U}}{dx_2}&=0 \end{aligned} \tag{45}$$

(c) Section Three

Section three is the joint region and includes the tapered portion of the lower and upper adherends and the adhesive. The equilibrium equations for the lower and upper laminates are obtained from a force and moment balance.

$$\frac{dN^{L}}{dx_3} = -\frac{p_x}{\cos\theta} \tag{46}$$

$$\frac{dQ^{L}}{dx_3} = -\frac{p_z}{\cos\theta} \tag{47}$$

$$\frac{dM^{L}}{dx_3} = k^{L} A_{55}^{L}\left(\psi_3^{L} + \frac{dw_3^{L}}{dx_3}\right) - \frac{N^{L}\tan\theta}{2} - p_x\left(\frac{l - x_3}{2}\right)\frac{\tan\theta}{\cos\theta} \tag{48}$$

$$\frac{dN^{U}}{dx_3} = \frac{p_x}{\cos\theta} \tag{49}$$

$$\frac{dQ^{U}}{dx_3} = \frac{p_z}{\cos\theta} \tag{50}$$

$$\frac{dM^{U}}{dx_3} = k^{U} A_{55}^{U}\left(\psi_3^{U} + \frac{dw_3^{U}}{dx_3}\right) - \frac{N^{U}\tan\theta}{2} - p_x\frac{x_3\tan\theta}{\cos\theta} \tag{51}$$

where p_x and p_z, see Fig. 5, are combinations of projections of the adhesive stresses from the vertical and horizontal surfaces to the inclined taper surface for the taper area corresponding to dx. From Fig. 6, the relations among p_x, p_z, σ_x, σ_z, and τ_{xz} are

$$\begin{aligned} p_x &= \sigma_x \sin\theta + \tau_{xz}\cos\theta \\ p_z &= \sigma_z \cos\theta + \tau_{xz}\sin\theta \end{aligned} \tag{52}$$

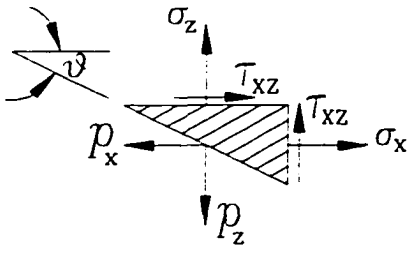

Figure 6 Adhesive Stresses - Laminated Plate Model

and the adhesive stresses σ_x, σ_z and τ_{xz} can be related to the adhesive mechanical properties and the laminate displacement field as

$$\sigma_x = E\frac{\partial u}{\partial x} = \frac{E\,(u^U - u^L)}{s}$$

$$\sigma_z = E\frac{\partial w}{\partial z} = \frac{E\left(w^U - s\left(\frac{dw^U}{dx}\right) - w^L\right)}{s\tan\theta} \qquad (53)$$

$$\tau_{xz} = G\left(\frac{\partial u}{\partial z} + \frac{\partial w}{\partial x}\right) = G\left(\frac{u^U - s\left(\frac{\partial u^U}{\partial x}\right) - u^L}{s\tan\theta} + \frac{w^U - w^L}{s}\right)$$

where E and G are the Young's and shear modului of the adhesive, s is the horizontal distance across the adhesive, and the displacement variables, u and w, are defined in Eqs. (28) and (29). Combining these equations with Eqs. (32)-(35) and Eqs. (41)-(42) yields the governing equations of the model. Substituting into these equations, and noting that $[A]$, $[B]$ and $[D]$ are functions of x in this section because of the taper, yields the governing equations.

$$A_{11}^{L}\frac{d^2u_3^{oL}}{dx_3^2}+\frac{dA_{11}^{L}}{dx_3}\frac{du_3^{oL}}{dx_3}+B_{11}^{L}\frac{d^2\psi_3^{L}}{dx_3^2}+\frac{dB_{11}^{L}}{dx_3}\frac{d\psi_3^{L}}{dx_3}=-\frac{p_x}{\cos\theta} \tag{54}$$

$$\begin{aligned}&B_{11}^{L}\frac{d^2u_3^{oL}}{dx_3^2}+\frac{dB_{11}^{L}}{dx_3}\frac{du_3^{oL}}{dx_3}+D_{11}^{L}\frac{d^2\psi_3^{L}}{dx_3^2}+\frac{dD_{11}^{L}}{dx_3}\frac{d\psi_3^{L}}{dx_3}\\&=k^{L}A_{55}^{L}\left(\psi_3^{L}+\frac{dw_3^{L}}{dx_3}\right)-\frac{N^{L}\tan\theta}{2}-p_x\left(\frac{l-x_3}{2}\right)\frac{\tan\theta}{\cos\theta}\end{aligned} \tag{55}$$

$$k^{L}\frac{dA_{55}^{L}}{dx_3}\left(\psi_3^{L}+\frac{dw_3^{L}}{dx_3}\right)+k^{L}A_{55}^{L}\left(\frac{d\psi_3^{L}}{dx_3}+\frac{d^2w_3^{L}}{dx_3^2}\right)=-\frac{p_z}{\cos\theta} \tag{56}$$

$$A_{11}^{U}\frac{d^2u_3^{oU}}{dx_3^2}+\frac{dA_{11}^{U}}{dx_3}\frac{du_3^{oU}}{dx_3}+B_{11}^{U}\frac{d^2\psi_3^{U}}{dx_3^2}+\frac{dB_{11}^{U}}{dx_3}\frac{d\psi_3^{U}}{dx_3}=\frac{p_x}{\cos\theta} \tag{57}$$

$$\begin{aligned}&B_{11}^{U}\frac{d^2u_3^{oU}}{dx_3^2}+\frac{dB_{11}^{U}}{dx_3}\frac{du_3^{oU}}{dx_3}+D_{11}^{U}\frac{d^2\psi_3^{U}}{dx_3^2}+\frac{dD_{11}^{U}}{dx_3}\frac{d\psi_3^{U}}{dx_3}\\&=k^{U}A_{55}^{U}\left(\psi_3^{U}+\frac{dw_3^{U}}{dx_3}\right)-\frac{N^{U}\tan\theta}{2}-p_x\frac{x_3\tan\theta}{2\cos\theta}\end{aligned} \tag{58}$$

$$k^{U}\frac{dA_{55}^{U}}{dx_3}\left(\psi_3^{U}+\frac{dw_3^{U}}{dx_3}\right)+k^{U}A_{55}^{U}\left(\frac{d\psi_3^{U}}{dx_3}+\frac{d^2w_3^{U}}{dx_3^2}\right)=\frac{p_z}{\cos\theta} \tag{59}$$

These six second-order equations can be reduced to a set of twelve first-order equations that can be combined with Eqs. (44) and (45) to yield the overall model of the assembly. The overall model has three first-order equations in region one for u_1^{oL}, ψ_1^{L} and w_1^{L}, three first-

order equations in region two for u_2^{oU}, ψ_2^U, and w_2^U, and six first-order equations for u^{oL}, du^{oL}/dx, ψ^L, $d\psi^L/dx$, w^L and dw^L/dx for the lower laminate in the joint region and six similar equations for the upper laminate in the joint region. The resulting eighteen simultaneous, linear, coupled, first-order differential equations with variable coefficients must be solved numerical subject to the following boundary conditions. Since there are eighteen equations in the model, eighteen boundary conditions or equations are required. The system of equations are integrated from left to right. The left end of the assembly is assumed to be pinned which results in the following conditions:

$$u_1^{oL} = 0 \tag{60}$$

$$w_1^L = 0 \tag{61}$$

At the right end of the assembly the laminate is assumed to be restrained in the z direction:

$$w_2^U = 0 \tag{62}$$

At each end of the joint region, continuity of each of the variables is assumed:

$$u_1^{oL} = u_3^{oL} \tag{63}$$

$$\psi_1^L = \psi_3^L \tag{64}$$

$$w_1^L = w_3^L \tag{65}$$

$$u_3^{oU} = u_2^{oU} \tag{66}$$

$$\psi_3^U = \psi_2^U \tag{67}$$

$$w_3^U = w_2^U \tag{68}$$

$$N^L = P \tag{69}$$

$$M^L = -Pw_3^L \tag{70}$$

$$Q^L = -P\frac{dw_3^L}{dx_3} \tag{71}$$

At the left end of the joint region, the following equations are enforced: Similar conditions apply at the right end of the joint:

$$N^U = P \tag{72}$$

$$M^U = -Pw_3^U \tag{73}$$

$$Q^U = -P\frac{dw_3^U}{dx_3} \tag{74}$$

These are fifteen boundary conditions and three additional conditions are needed to integrate tthe system of eighteen equations. At the left end of the joint the normal stress and moment resultants of the upper laminate are set to zero and at the right end of the joint the moment resultant of the lower laminate is set to zero.

$$N^{U}|_{x_3=0} = 0; \quad M^{U}|_{x_3=0} = 0; \quad M^{L}|_{x_3=l} = 0 \tag{75}$$

Intuitively, four conditions on the normal stress resultants are available. However, the normal stress resultants are governed by Eqs. (46) and (49). The right-hand sides of these equations have the same magnitude but opposite signs. Once the three conditions regarding N^U and N^L in Eqs. (69), (70), (72), (73) and (75) are satisfied, $N^L(l)$ will automatically equal zero. Therefore, only three of the conditions are independent and can be used to complete the solution. These eighteen values and equations are sufficient to numerically solve the model.

A FORTRAN program was developed on an IBM compatible personal computer to numerically solve the model. The Linear Shooting Method as described by Press, *et al.* [54] was chosen to integrate the system of equations. The fourth-order Runge-Kutta Method was chosen to carry out the integration of the equations. In the first and last step of the joint region, the Modified Euler Method was used to average the effect of the singularity [55] that occurs at each end of the joint where one of the adherends tends to zero cross-sectional area, and therefore, zero values of the equivalent moduli terms. The shooting method converts a two-point boundary problem to an iteratively solved initial value problem. Some of the known or assumed boundary conditions are specified at each end of the joint assembly. The unspecified variables at the left end of the assembly or joint can be adjusted to achieve the conditions at the right end of the joint and assembly. The equations are then integrated and the final conditions are checked. An algorithm is used to adjust the

unspecified initial conditions and the integration is repeated. The process is continued until the errors in the final conditions are small.

CHAPTER 4

CYLINDRICAL BENDING

Cylindrical bending occurs under four-point loading. The mid-plane of the laminate is bent into a cylindrical surface. Figure 7 is a pictorial representation of a laminated plate with a taper-taper joint bent into a cylindrical form by four-point loading.

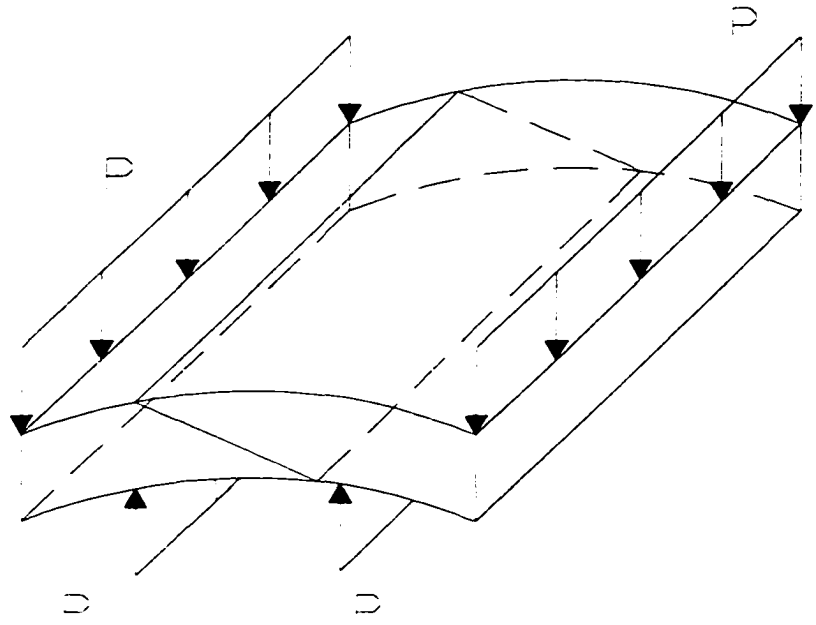

Figure 7 Plate Under Cylindrical Bending

The model derived in this research for the case of cylindrical bending was a one dimensional approximation of the case shown in Fig. 7. The one dimensional representation of the plate is shown in Fig. 8. The derivation of the model for cylindrical bending closely follows the development of the tension model. The applicable figures and equations in Chapter 3 will be referenced in the discussion below.

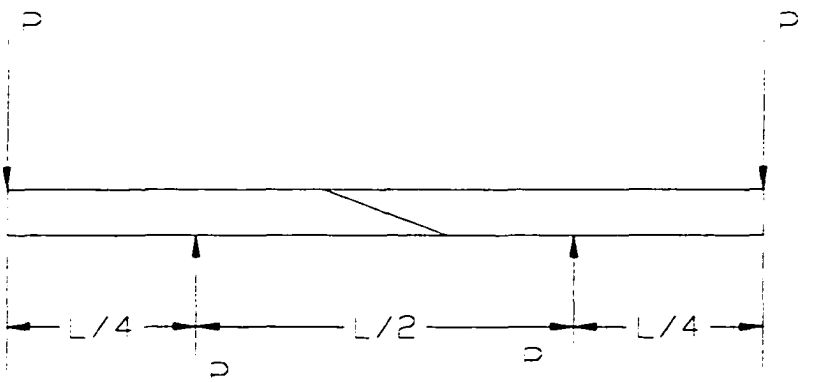

Figure 8 Joint Under Cylindrical Bending

The freebody diagram in Fig. 5 was used in the derivation of the model. For the lower and upper laminates, the thin slices shown in the figure were assumed to be in equilibrium. Stress resultants were summed in the horizontal and vertical directions and moments were summed about the center of the laminate slices to generate the equilibrium equations..

The displacements in the x and z directions are given in Eqs. (28)-(29). Using these equations the normal and shear strains can be expressed by Eqs. (30)-(31). The equations relating the normal stress and bending moment resultants to the plate displacements and equivalent moduli are given in Eqs. (32)-(35). The definitions of the equivalent moduli terms for the lower and upper laminates are given by Eqs. (36)-(37). The constitutive relation in Eq. (38) relates the shear stress resultant to the shear strain. The same value of the shear correction factors was chosen for this model, $k^L = k^U = 5/6$. The equivalent shear moduli for the lower and upper laminate are presented in Eqs. (39)-(40). These relations correlate the forces and moments in the laminate with the displacement field in terms of the equivalent modulus matrices.

Under cylindrical bending the joint area is subject to a constant applied moment. Summing forces in the horizontal and vertical directions and summing moments about the element center yields Eqs. (46)-(51). The adhesive relations are listed in Eq. (53). Combining the equations above with Eqs. (32)-(35) and Eqs. (41)-(42) yields the governing equations of the model which are listed in Eqs. (54)-(59). These six second-order ordinary differential equations with variable coefficients must be solved simultaneously subject to the boundary conditions listed below. To facilitate the solution, an order reduction method was employed to reduce the problem to a system of twelve, first-order equations.

Twelve boundary equations or values must be specified to solve the system of twelve linear, ordinary, first-order differential equations with variable coefficients. These equations and values are outlined and discussed below.

Since the stresses and strains are related to the derivatives of the variables u^o, ψ, and w, the datum for these variables are irrelevant. Therefore, these variables for the lower laminate were set to zero at $x = 0$.

$$\begin{aligned} u^{oL}(0) &= 0 \\ \psi^{L}(0) &= 0 \\ w^{L}(0) &= 0 \end{aligned} \tag{76}$$

Under four-point bending, the axial stress resultants must be zero at each end of the joint. Three of the four resultants are set to zero.

$$N^L(0) = A_{11}^L \frac{du^{oL}(0)}{dx} + B_{11}^L \frac{d\psi^L(0)}{dx} = 0$$

$$N^L(l) = A_{11}^L \frac{du^{oL}(l)}{dx} + B_{11}^L \frac{d\psi^L(l)}{dx} = 0 \qquad (77)$$

$$N^U(0) = A_{11}^U \frac{du^{oU}(0)}{dx} + B_{11}^U \frac{d\psi^U(0)}{dx} = 0$$

The right hand side of Eqs. (54) and (57), which govern the axial force resultants on the lower and upper laminates, have the same magnitude, but opposite sign. Once the three conditions above are satisfied, $N^U(l)$ will automatically be zero. Therefore, $N^U(l) = 0$ is not an independent boundary condition. The applied moment, M_o, is taken by the lower laminate at $x = 0$, and by the upper laminate at $x = l$. Therefore the following conditions are imposed.

$$M^L(0) = B_{11}^L \frac{du^{oL}(0)}{dx} + D_{11}^L \frac{d\psi^L(0)}{dx} = M_o$$

$$M^L(l) = B_{11}^L \frac{du^{oL}(l)}{dx} + D_{11}^L \frac{d\psi^L(l)}{dx} = 0$$

$$M^U(0) = B_{11}^U \frac{du^{oU}(0)}{dx} + D_{11}^U \frac{d\psi^U(0)}{dx} = 0 \qquad (78)$$

$$M^U(l) = B_{11}^U \frac{du^{oU}(l)}{dx} + D_{11}^U \frac{d\psi^U(l)}{dx} = M_o$$

Two additional boundary conditions are needed to solve the model. The shear resultants are zero at each end of the joint, but the conditions are not independent by an argument similar to that given above for the axial stress resultants. Two of these conditions are set

to equal to zero:

$$Q^{L}(l) = k^{L}A_{55}^{L}\left(\psi^{L}(l) + \frac{dw^{L}(l)}{dx}\right) = 0$$
$$Q^{U}(0) = k^{U}A_{55}^{U}\left(\psi^{U}(0) + \frac{dw^{U}(0)}{dx}\right) = 0 \qquad (79)$$

The twelve conditions above are sufficient to solve the model. The FORTRAN program developed to solve the tension loading case in Chapter 3 was modified to integrate the laminated plate model for the case of cylindrical bending.

CHAPTER 5

MODEL VERIFICATION

Finite element analysis was not a major part of this work, but was only used to verify the accuracy of the developed models for tension and cylindrical bending. The mechanics of materials and laminated plate models were both verified for tension loading using finite element models constructed with the COSMOS/M finite element software [56]. The cylindrical bending laminated plate model was also verified using a COSMOS/M finite element model. The laminates modeled were relatively thin and the angles involved resulted in small surface areas in the joint region. The small surface areas of the joints precluded the use of strain gauges. At most, the strain at one point on the surface of the laminate in the joint region would have been obtainable. Finite element models were chosen for verification in order to generate a point-by-point comparison with the analytical models along the x-axis.

For the mechanics of materials model two plate thicknesses and two taper angles were modeled. The plates and adhesive were modeled using 2-D plane strain, four-noded quadrilateral elements. In the models, the first 0.8 mm of the sharp tapers was truncated to match the geometry used in the analytical model. Finite elements were generated using reduced integration for the case of plane strain. The details of the mesh in the joint region are shown in Fig. 9.

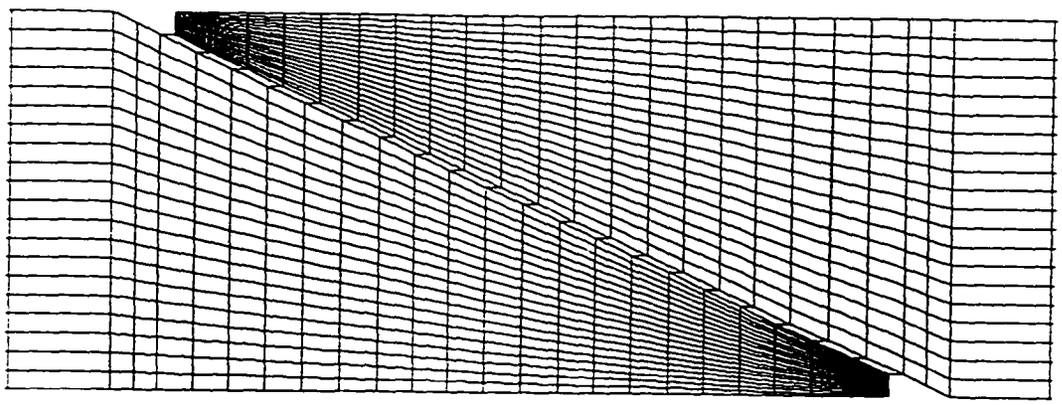

Figure 9 Finite Element Mesh - Mechanics of Materials Model

COSMOS/M models were used to verify the laminated plate model for a 20° taper angle and unidirectional and crossply laminates under tension. In these models the entire taper was included to match the laminated plate model. 2-D plane strain, eight-noded quadrilateral elements were used. The mesh consisted of 2,248 elements. The finite elements were generated using reduced integration for the case of plane strain. Figure 10 is a plot of the mesh used to model the joint region.

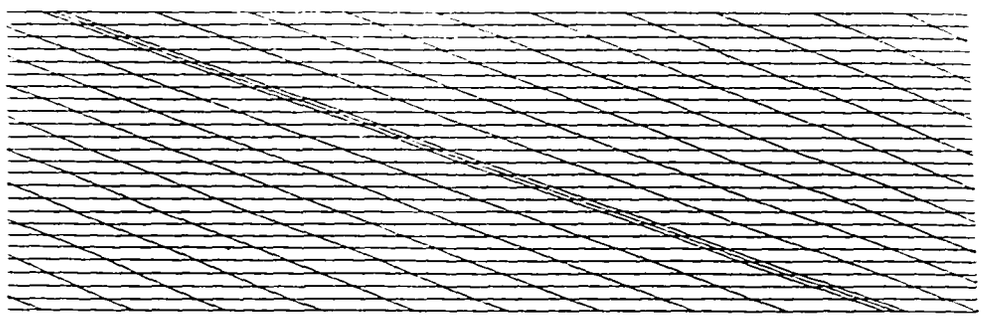

Figure 10 Finite Element Model for Laminated Plate Model Under Tension

The finite element models used in the tension case were not adequate for the bending case. The model produced stresses that generally followed the model but had some sharp

excursions. This was caused by the rotation of the elements and the change of angles in the elements adjacent to the adhesive. To overcome this problem the model was meshed using constant angle elements that matched the taper angle in most of the model. The transition section was outside of the points of load application. A detail of the mesh is shown in Fig. 11. The model was meshed using a higher density of lower order elements than the tension model. The model used 5,376 four-noded quadrilateral elements. The 2-D plane strain elements were generated using reduced integration.

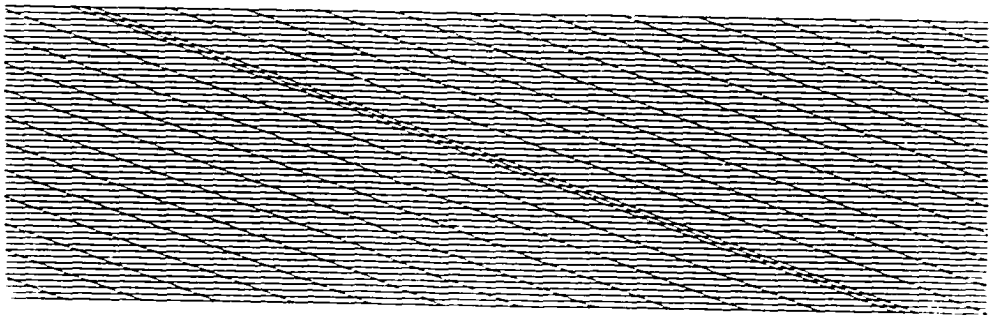

Figure 11 Finite Element Mesh for Laminated Plate Model Under Cylindrical Bending

CHAPTER 6

RESULTS AND DISCUSSION

6.1 Mechanics of Materials Model - Tension

Table 1 lists the properties that were used in the mechanics of materials and finite element models.

Table 1 Properties of Scotchply Plate

Property	Value
Modulus of elasticity for plate (GPa)	39.3 (Unidirectional) 24.5 (Crossply)
Thickness of plate (mm)	6.35 (Unidirectional) 3.175 (Crossply)
Shear modulus of adhesive (GPa)	0.34
Modulus of elasticity of adhesive (GPa)	0.96
Thickness of adhesive layer (mm)	0.084
Poisson's ratio for plate	0.3

The finite element results are superimposed on the analytical results in the four graphs included as Figs. 12 through 15. Figure 12 shows the strain distribution for 3.175 mm plate with a 15° taper angle, and Fig. 13 shows the strain distribution for the 3.175 mm plate with a 20° taper angle. The strain is nearly constant through most of the joint and falls toward zero as the end of the taper is approached. The finite element results match the analytical model closely except in the vicinity of the end of the taper where the strain

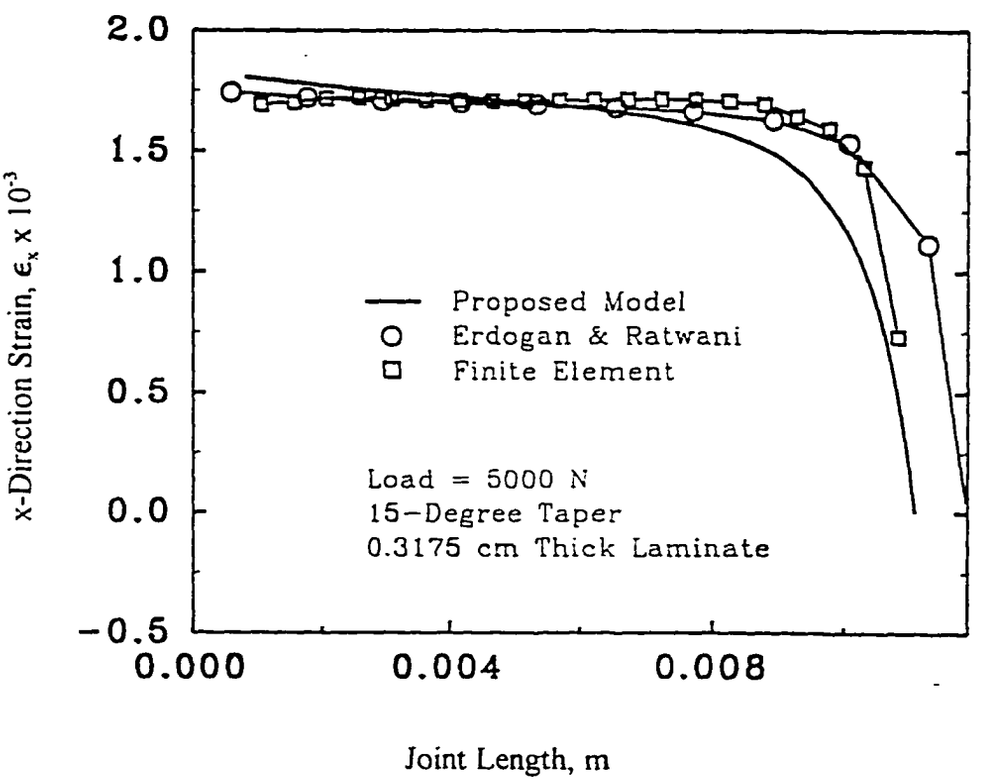

Figure 12 Strain Distribution for 3.175 mm Plate at 15°

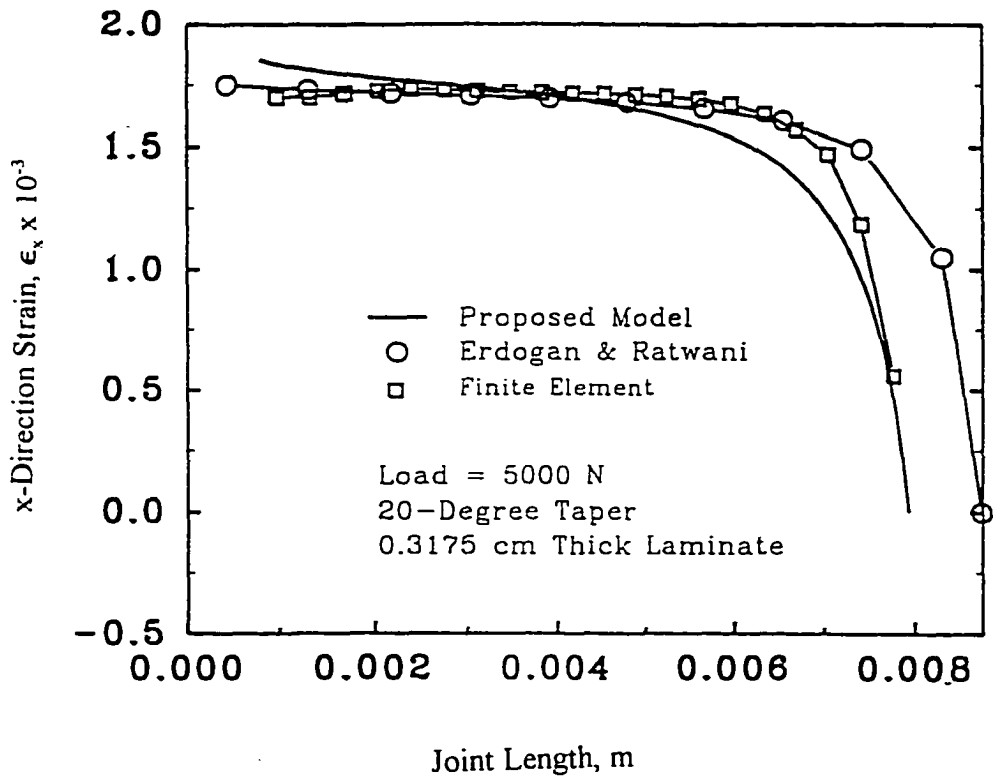

Figure 13 Strain Distrubution for 3.175 mm Plate at 20°

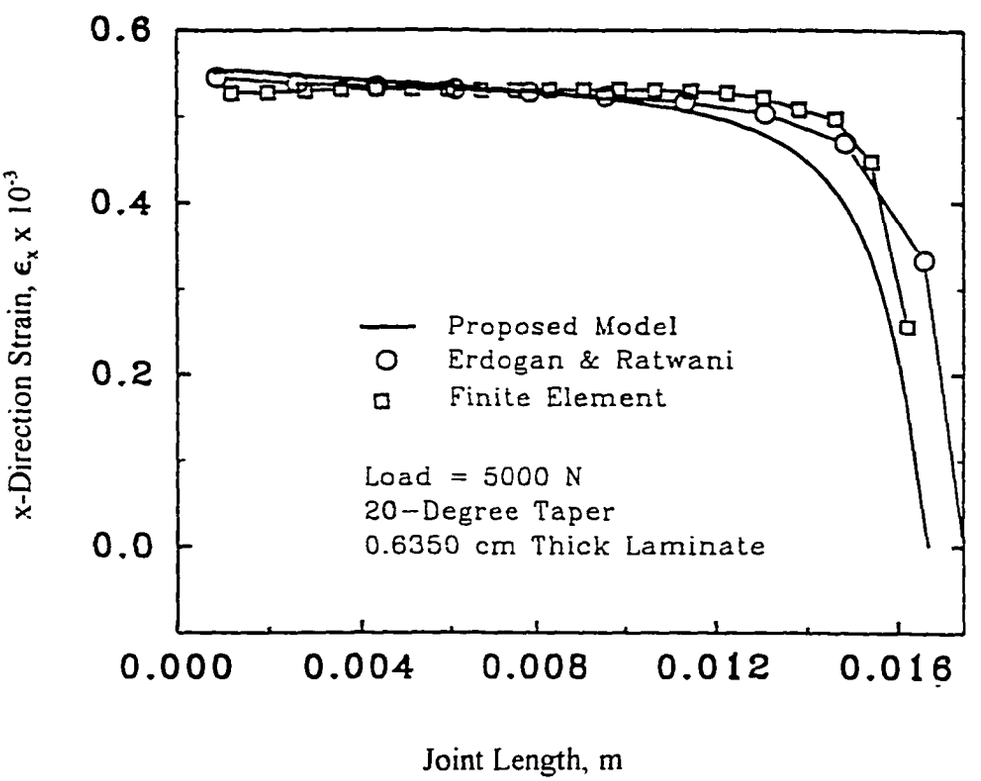

Figure 14 Strain Distribution for 6.35 mm Plate at 20°

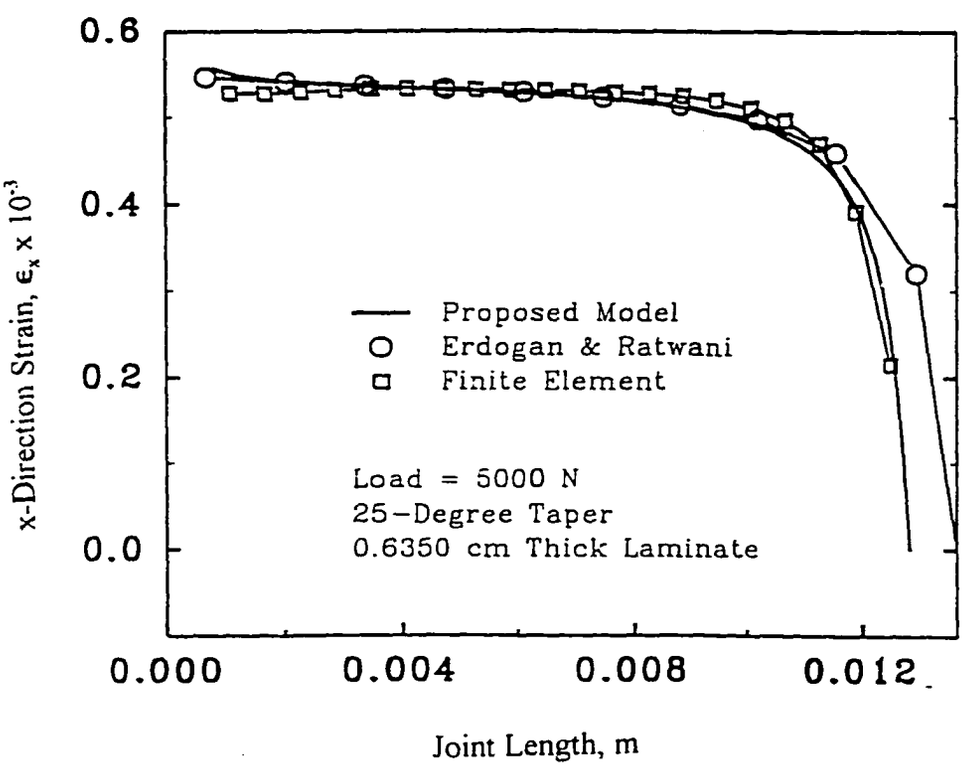

Figure 15 Strain Distribution for 6.35 mm Plate at 25°

falls to zero more quickly for the analytical model. This mismatch is probably due to the omission of the moment equations from the model. The finite element results are strains at the center of each element and therefore do not reach zero for the last element in the taper. The same situation occurs at the beginning of the taper. Figure 14 shows the strain along the joint length for the 6.35 mm plate with a 20° taper, and Fig. 15 shows the same for a 25° taper. The strains are again nearly constant along most of the joint. There is a slight mismatch near the end of the taper in Fig. 14, but the overall agreement is excellent in Fig. 15. The agreement improves with the thicker plate and the steeper angle because there is more material in the area near the end of the taper to resist the shear stresses caused by the taper. The calculated strains are smaller for the thicker plates because the same load was used for both plate thicknesses, and the thicker plates have more material to resist the load. The analytical model and the finite element model agree well and are within about 5 to 10% of each other over the length of the joint.

The method of Erdogan and Ratwani [47] was used to provide an additional check on the accuracy of the mechanics of materials model. The method is summarized briefly in Chapter 2, Eqs. (1)-(3). For comparison with the model and the finite element results, the joint was divided into ten steps and the strains were calculated at the center of each step. A personal computer program was written in the C computer language to evaluate the constants and calculate the strains. The data points extend beyond either end of the other models because there is no truncation of the ends of the joint in the stepped joint model. The stepped joint approximation data are superposed on Figs. 12-15. This model matches the analytical model well in the area away from the end of the taper and fits better for the

thicker plate and steeper angle. The model does not fit well near the end of the taper, as the cross-sectional area of the stepped joint does not go to zero. The stepped joint approximation would approach zero area at the last step if the number of steps became infinitely large.

6.2 Laminated Plate Model - Tension

A 16 ply unidirectional laminate of T300/5208 (Graphite/Epoxy) with ply thicknesses of 0.25 mm and a $[90_4/0_4/90_4/0_4]$ laminate of the same material were chosen for demonstration of the analytical model. Identical laminates were used in each case for the lower and upper adherends. The engineering constants of T300/5208 are [68] E_x = 181 GPa, E_y = 10.3 GPa, E_s = 7.17 GPa and ν_{xy} = 0.28. Table 2 lists the equivalent moduli per unit width for the laminates outside of the joint area.

Table 2 Equivalent Moduli for the Laminates

	A_{11}, MN	B_{11}, kNm	D_{11}, Nm^2	A_{55}, MN
Unidirectional	727	0	969.6	28.7
Crossply	384	-171.5	512	28.7

In the joint region the A_{11}, B_{11}, and D_{11} terms were represented algebracially as functions of x to account for the varying amount of material removed to machine the taper angle. Each laminate has a 50 mm long straight section on the end plus the tapered region whose length is a function of the taper angle. The tension load applied was 1,000 N/m.

The properties assumed for the elastic isotropic adhesive are listed in Table 3.

Table 3 Adhesive Properties

Modulus of Elasticity, E (GPa)	0.96
Shear Modulus, G (GPa)	0 .34

The shear correction factor was introduced by Reissner [9] and Mindlin [64] for isotropic plates. The choice of the shear correction factor k for anisotropic plates is not trivial. The value of the factor has been shown to depend on both laminate materials and stacking sequence. Several values have been suggested by researchers. A value of 5/6 was suggested by Whitney and Pagano [11], and the results were shown to be close to the exact solutions for a crossply laminate under bending. Calculations with two different k values (2/3 and 5/6) indicated that the model was not very sensitive to the shear correction factor. The adhesive stresses were almost identical for both values with a maximum difference of about 2% near the peak peel stress for the crossply case. Therefore, the value of k in Eqs. (44)-(45) and (54)-(59) was chosen as 5/6 to simulate both k^U and k^L.

A 20° taper angle was chosen for the examples presented in Figs. 16-25. The unidirectional results are shown in Figs. 16-20 and the crossply results are shown in Figs. 21-25. The results are shown for the joint region only. The distribution of the normal stress resultants are shown in Fig. 16. The plots are linear as expected for unidirectional material. The bending moment and shear resultants are shown in Figs. 17 and 18. The bending moments are zero at each end of the joint because there is no applied moment and the moment present within the joint is generated by the tapers. Figure 19 is the peel stress

distribution in the adhesive and Fig. 20 is the shear stress distribution in the adhesive. The results of the finite element model are superposed on the curves in Figs. 19 and 20. The agreement between the analytical model and the finite element model is very good with only a slight mismatch near the ends of the joint. The adhesive stresses are very uniform as expected since the adherends have uniform properties in the x-direction [44]. The normal stress resultant, bending moment, and shear resultant are shown in Figs. 21-23 for the crossply case. The normal resultants are not linear for the crossply case. This is due to the different properties of the ply groups. The bending moments are both zero at each end of the joint due to the absence of any applied moments. The shear resultant curves show local maximums at the ply group interfaces where there is a discontinuity of properties. The adhesive peel and shear stresses are shown in Figs. 24-25. In Fig. 24 the peel stress curves are similar. The maximum peel stress occurs at about x/l=0.4 and the mismatch between the two curves is only about 5%. In Fig. 25 the shear stress curves are also similar. The maximum shear stress occurs at about x/l=0.3 and the mismatch is about 8%. This agreement between the analytical model and the finite element model is good and should be usable for future failure analysis. The stresses are not uniform due to the change in properties between ply groups. It is interesting to note that the second ply group takes most of the load, followed by the bottom ply. This is as expected since the 0° ply groups have significantly more strength in the x-direction than the 90° ply groups.

Figures 26-27 are plots of the adhesive peel and shear stresses for the unidirectional laminate with two different values of the shear correction factor. Figures 28-29 are similar

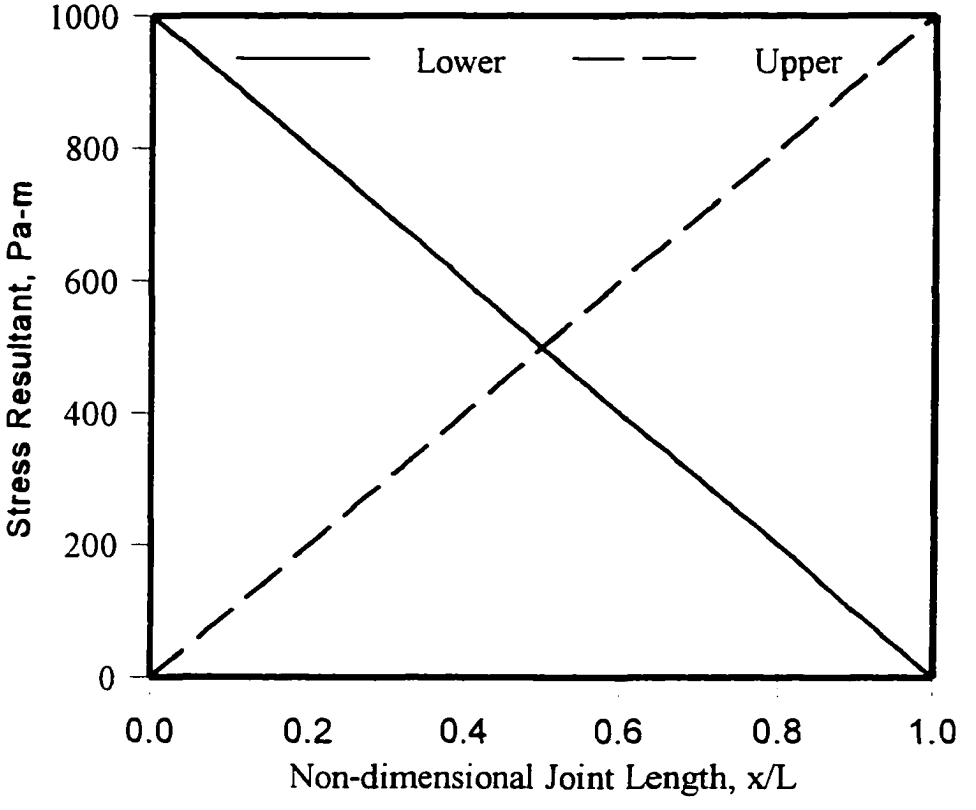

Figure 16 Normal Stress Resultant in *x* Direction - Unidirectional

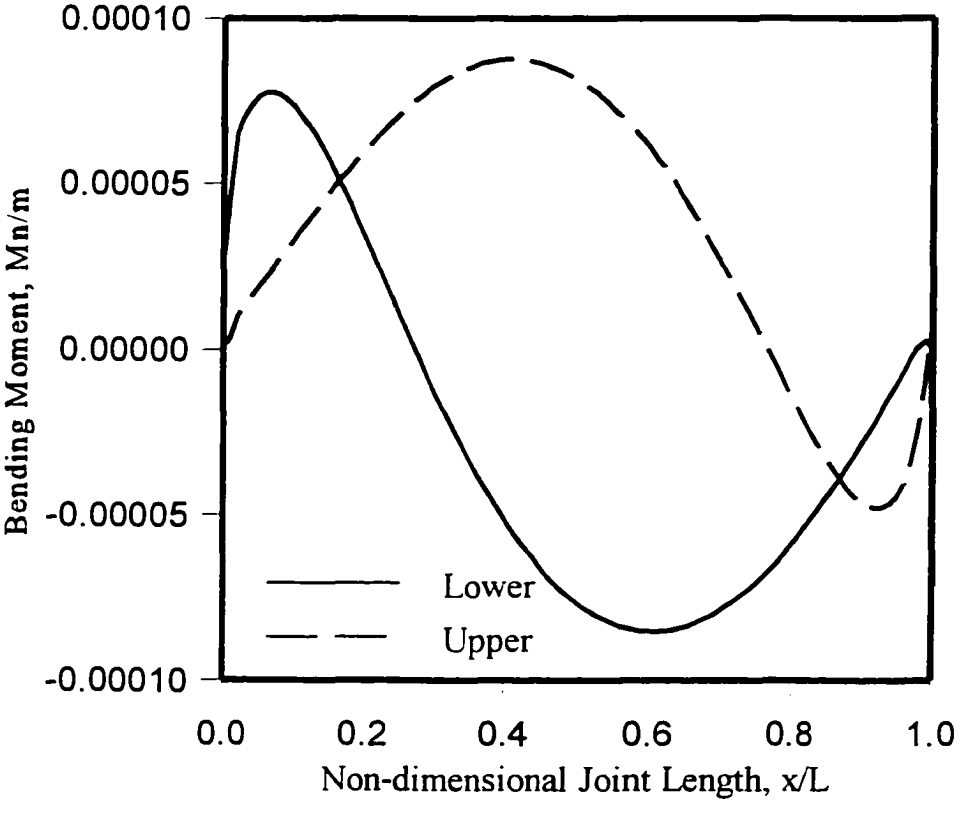

Figure 17 Bending Moment Resultant - Unidirectional

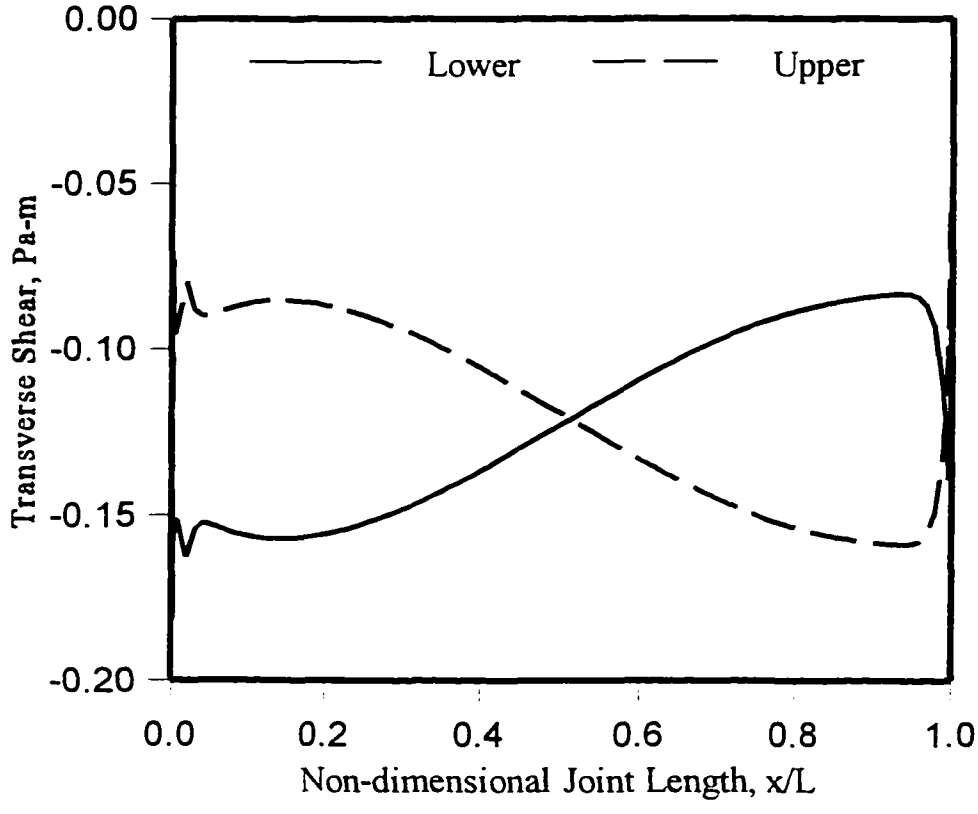

Figure 18 Shear Stress Resultant - Unidirectional

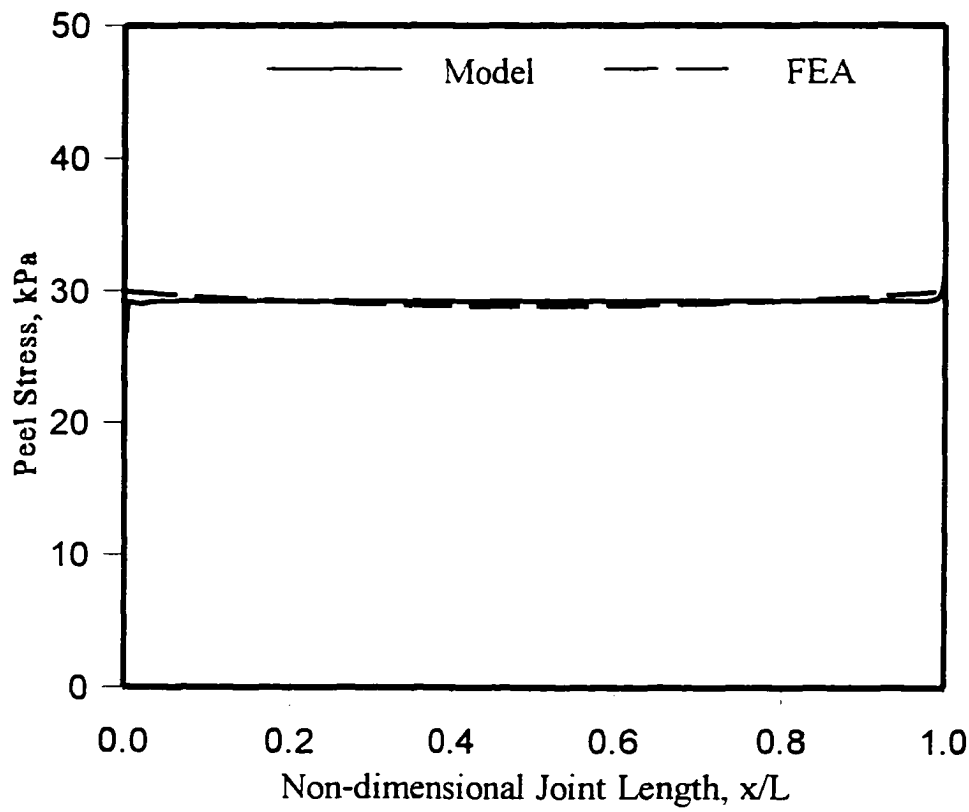

Figure 19 Adhesive Peel Stress - Unidirectional

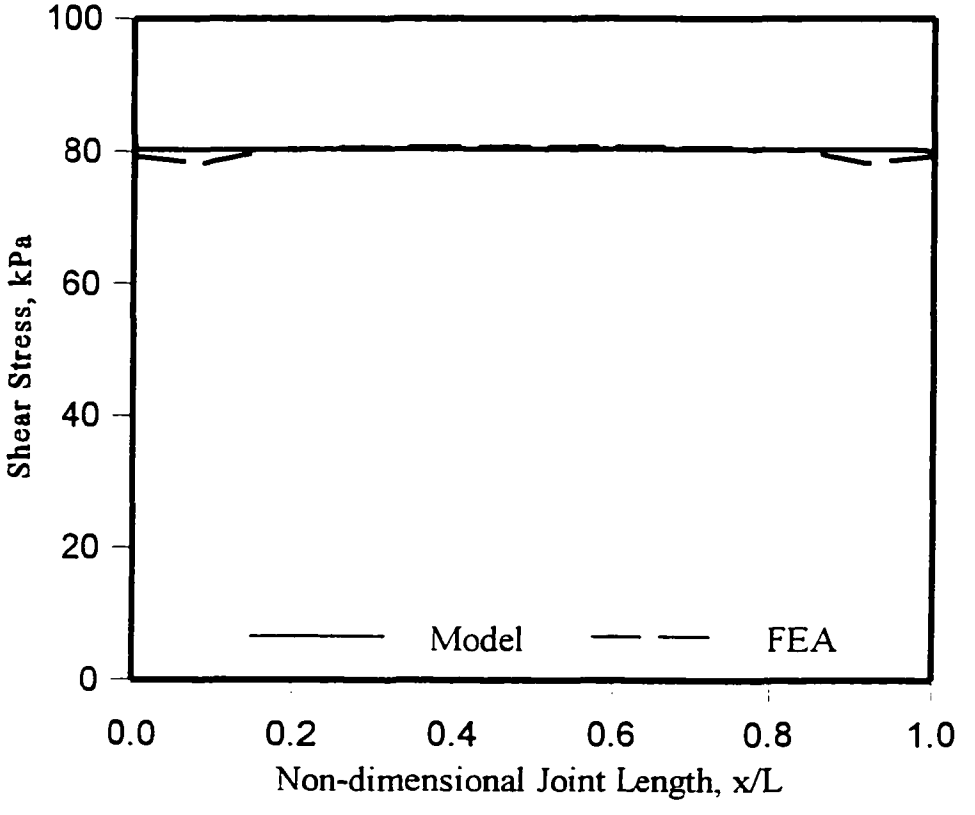

Figure 20 Adhesive Shear Stress - Unidirectional

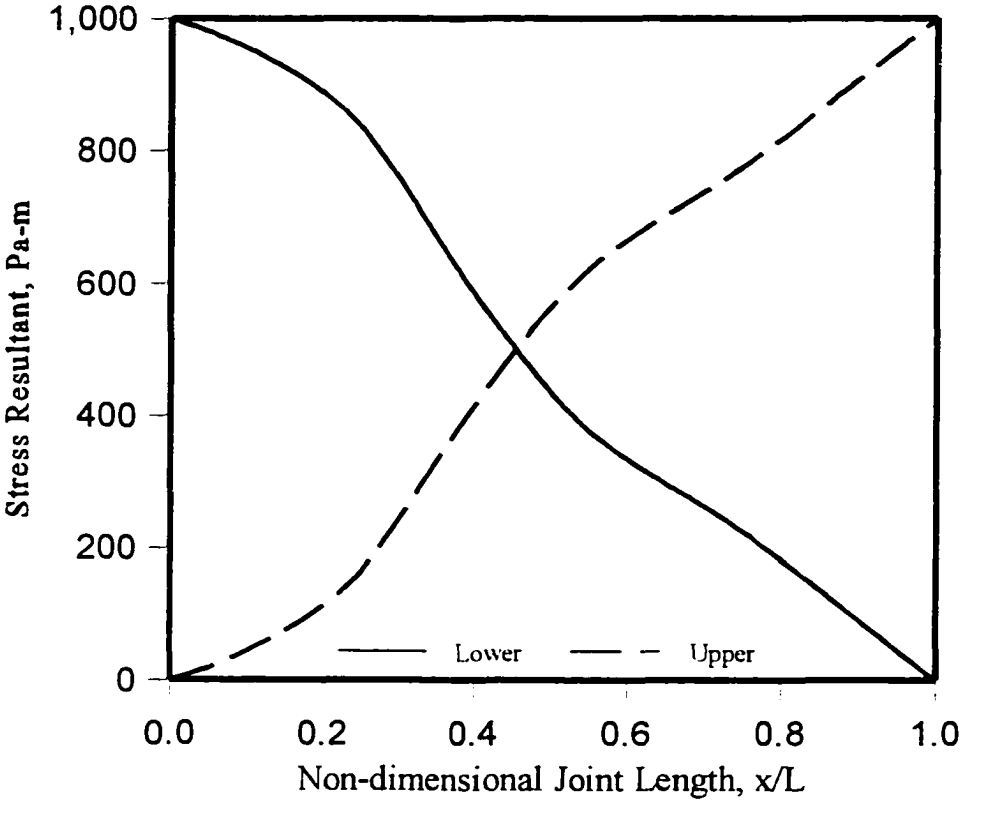

Figure 21 Normal Stress Resultant in *x* Direction - Crossply

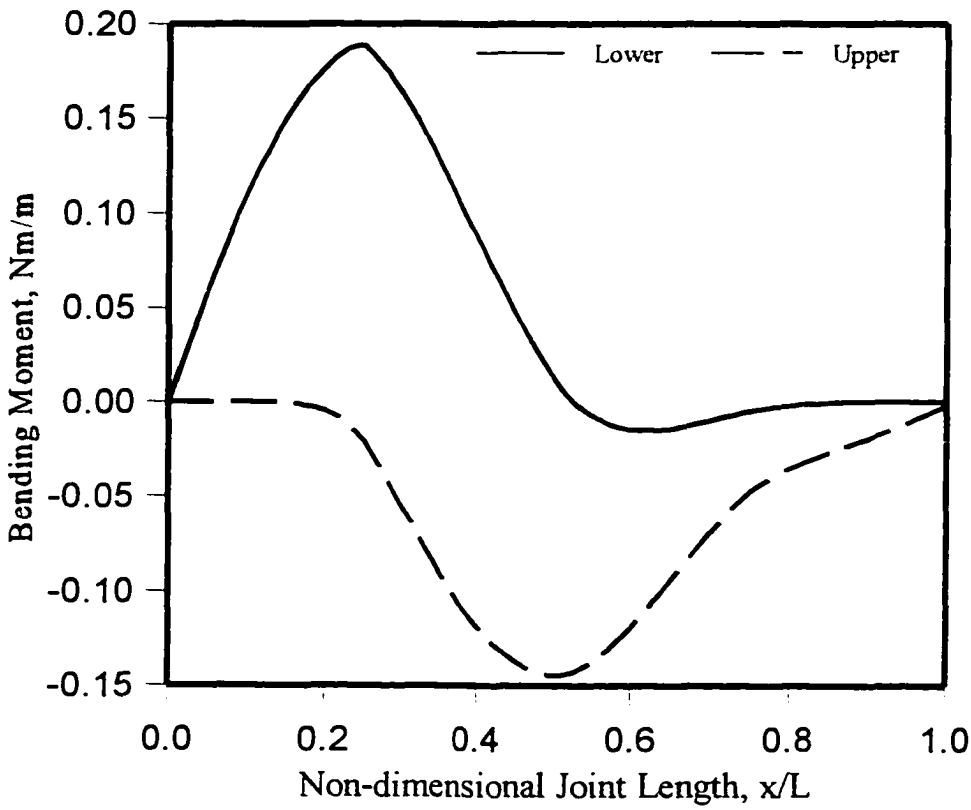

Figure 22 Bending Moment Resultant - Crossply

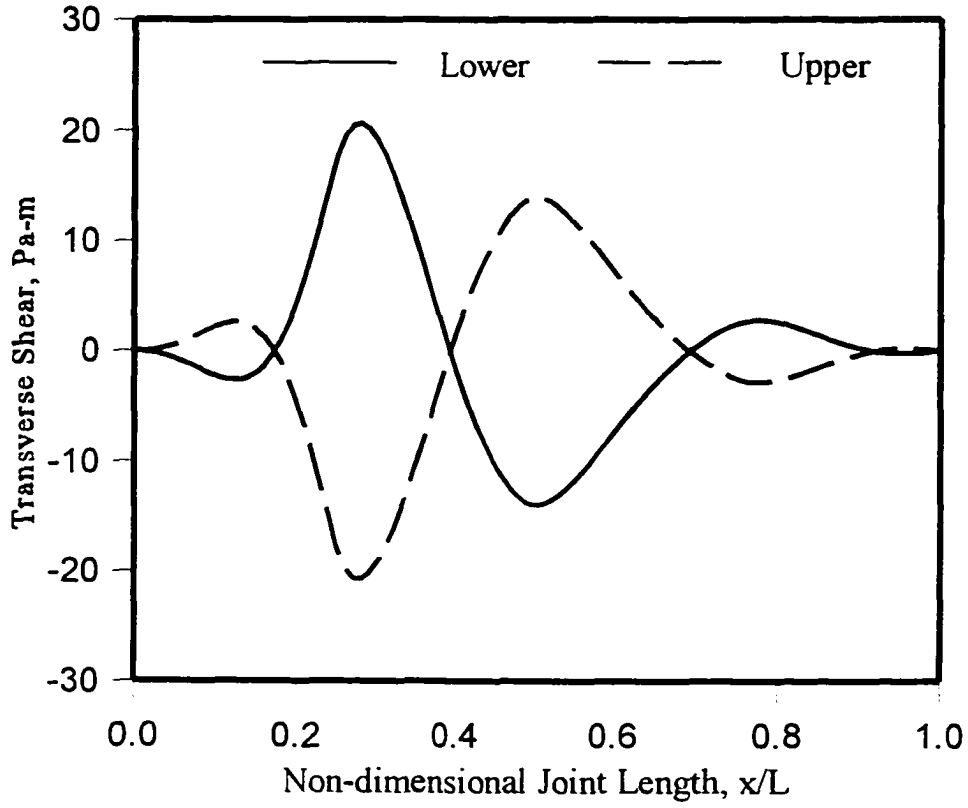

Figure 23 Shear Stress Resultant - Crossply

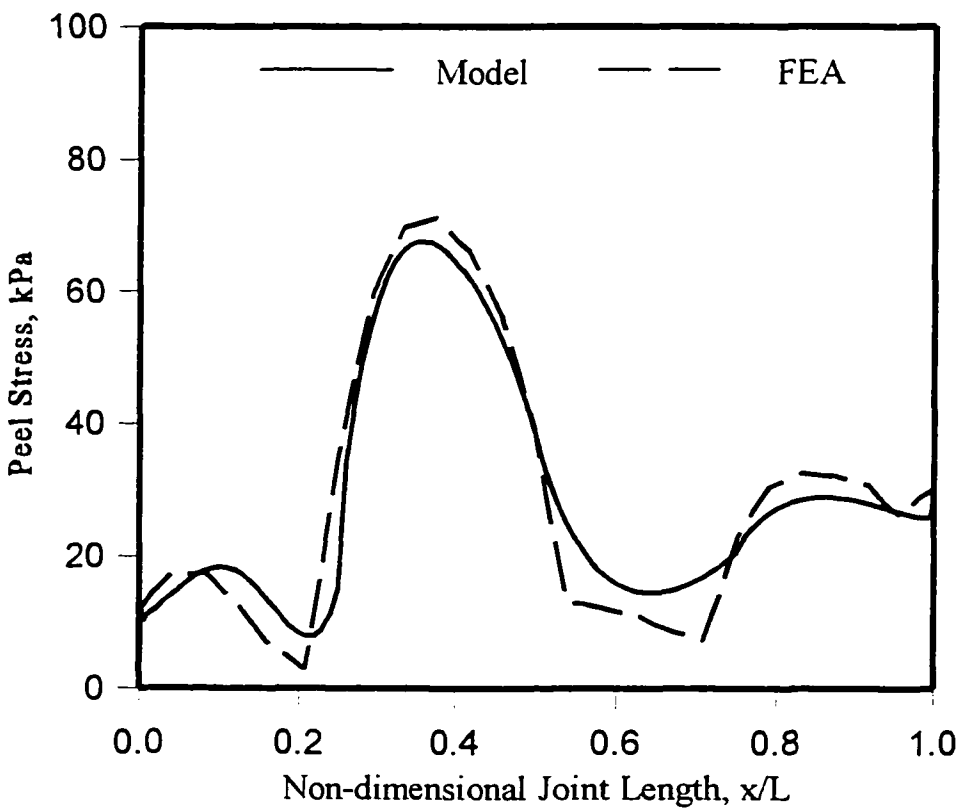

Figure 24 Adhesive Peel Stress - Crossply

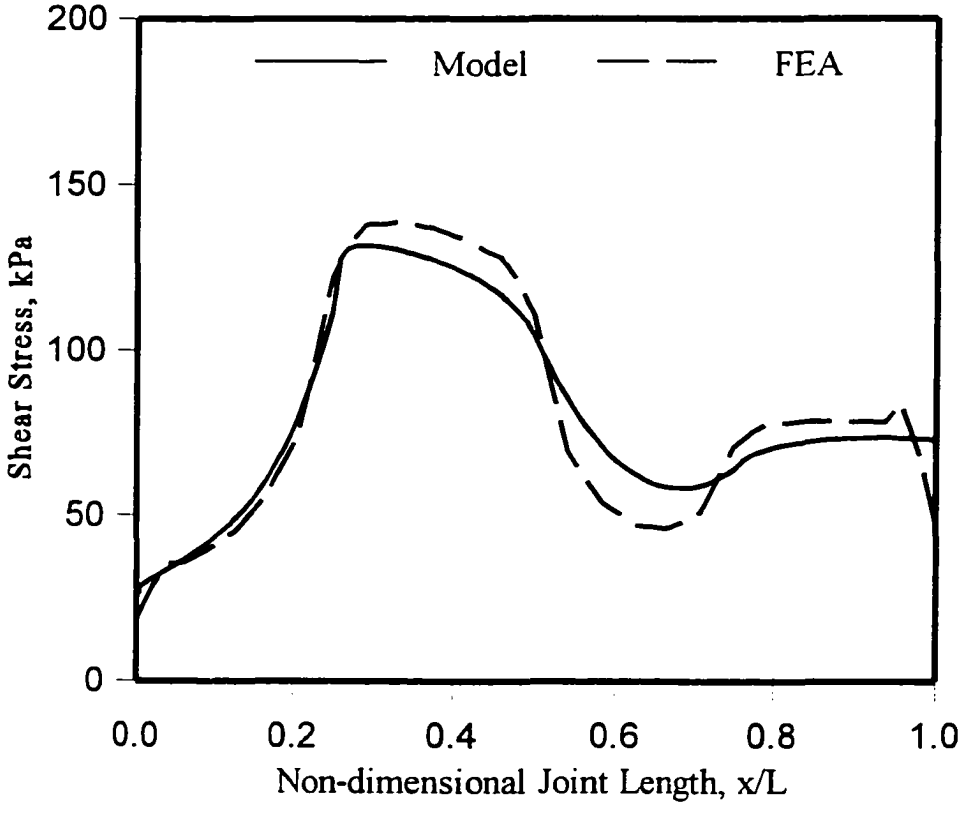

Figure 25 Adhesive Shear Stress - Crossply

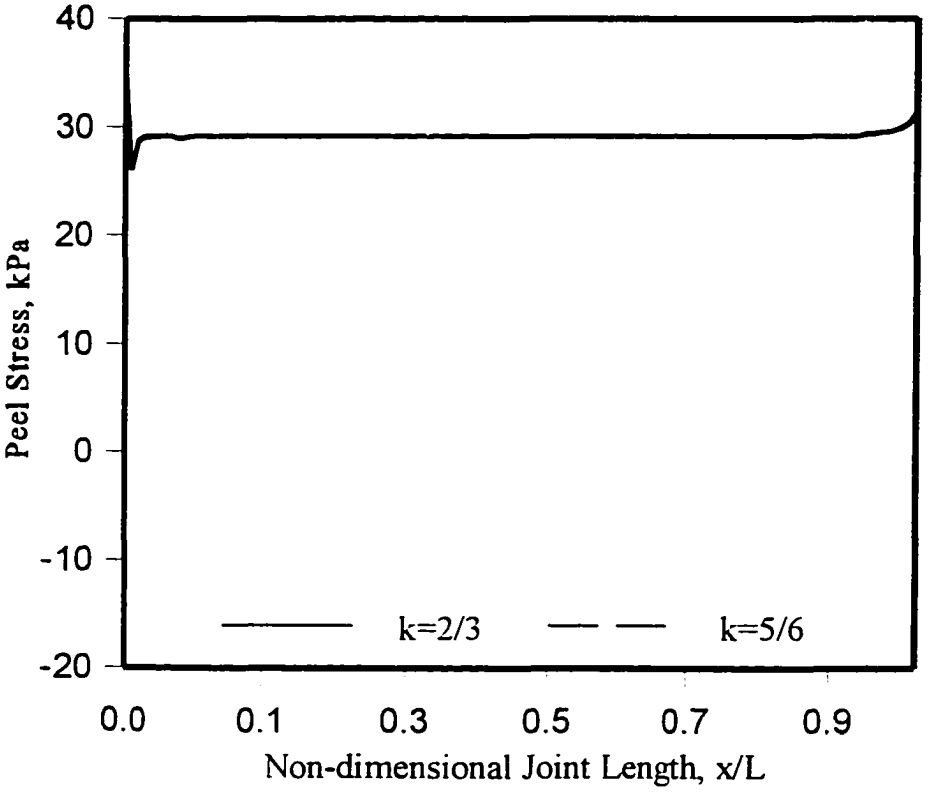

Figure 26 Adhesive Peel Stress as a Function of k for Unidirectional Laminate

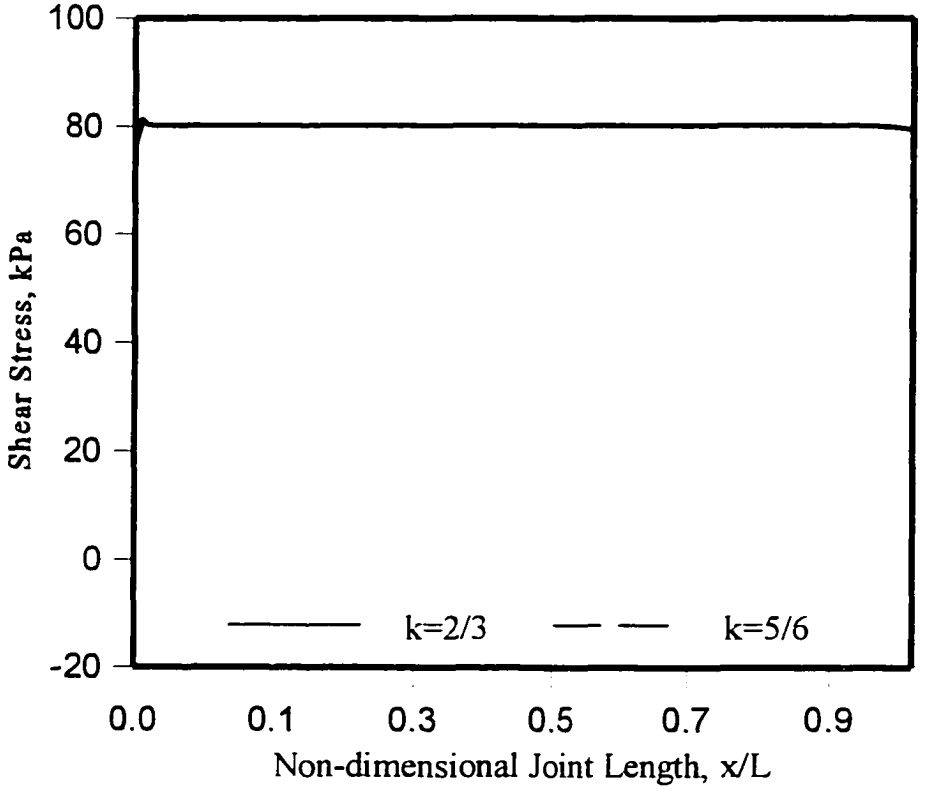

Figure 27 Adhesive Shear Stress as a Function of k for Unidirectional Laminate

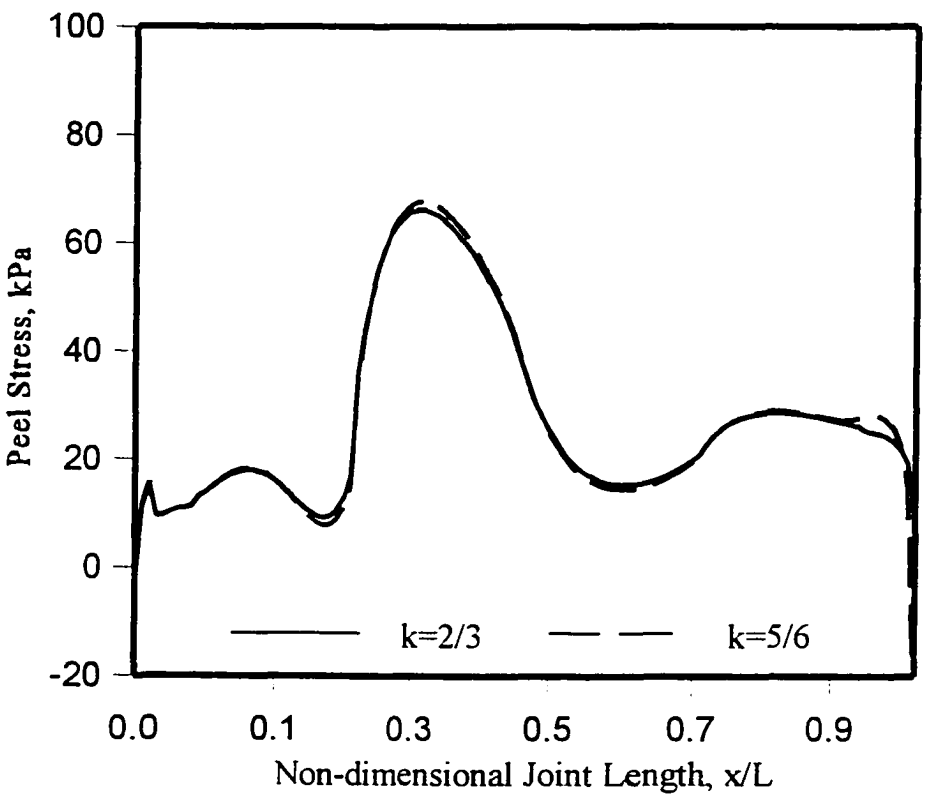

Figure 28 Adhesive Peel Stress as a Function of k for Crossply Laminate

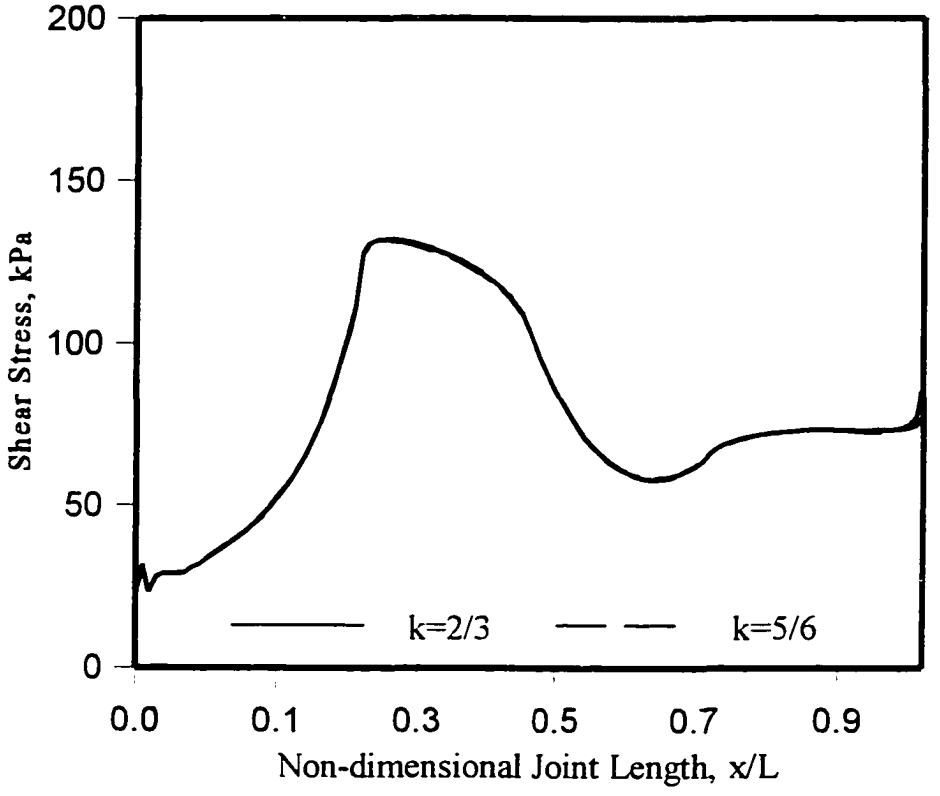

Figure 29 Adhesive Shear Stress as a Function of k for Crossply Laminate

plots for the crossply laminate. All four plots show that the model is not very sensitive to the value of the shear correction as noted above.

6.3 Laminated Plate Model - Bending

The applied bending moment was 2 Nm. Figure 30 is the distribution of the normal stress resultants. The curves for the lower and upper laminate are symmetric about the x-axis and start and end at zero because there is no in-plane load applied to the laminate. Figure 31 is the bending moment resultant. The moment resultant equals the applied moment at the left end of the joint for the lower laminate and at the right end of the upper laminate. Figure 32 is the shear stress resultant. The plots are symmetric about the x-axis and have stress reversals at the ply interfaces. Figure 33 is the adhesive peel stress distribution.The highest stresses are carried by the adhesive adjacent to the two 0° ply groups as expected. The peak stresses are within about 2% of those predicted by the finite element analysis results. Figure 34 is the adhesive shear stress distribution. The peak stresses are also carried by the adhesive adjacent to the two 0° ply groups. The peak stresses predicted by the analytical model are very close to the finite element analysis results.

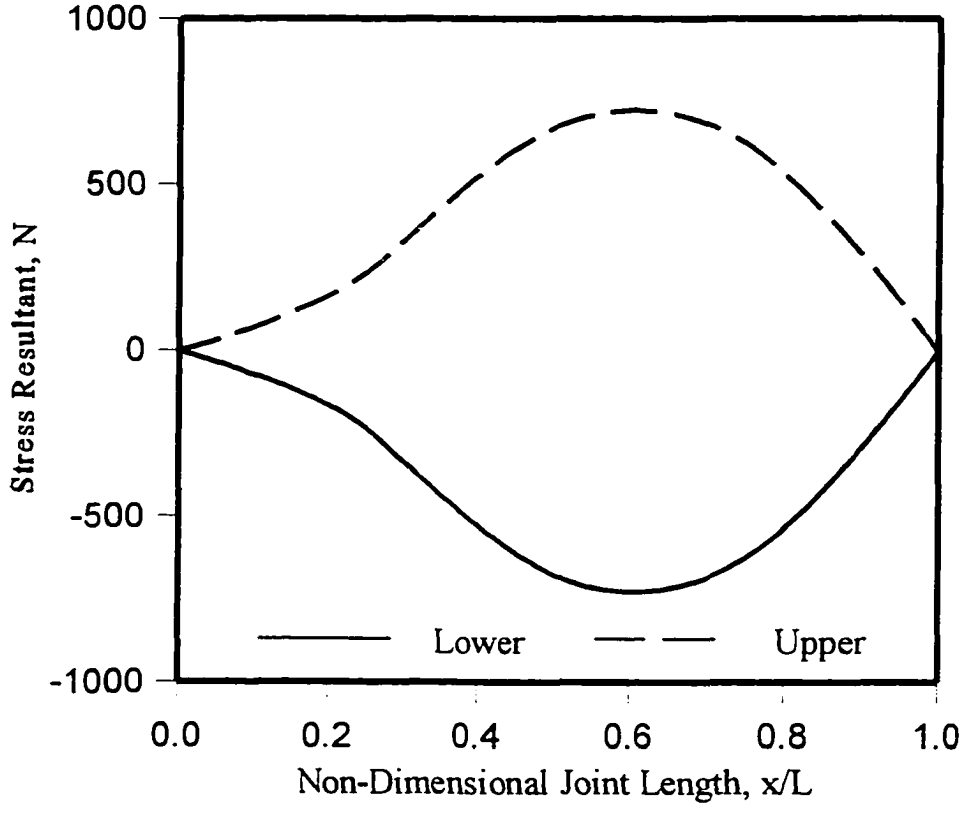

Figure 30 Normal Stress Resultant in *x*-Direction - Crossply

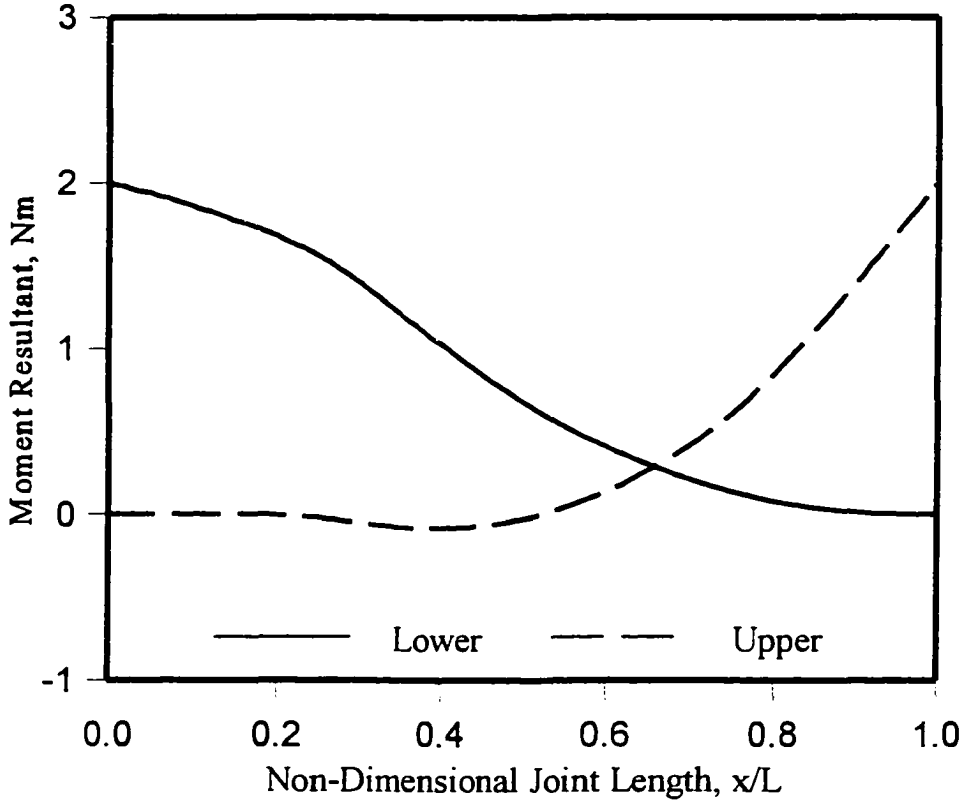

Figure 31 Bending Moment Resultant - Crossply

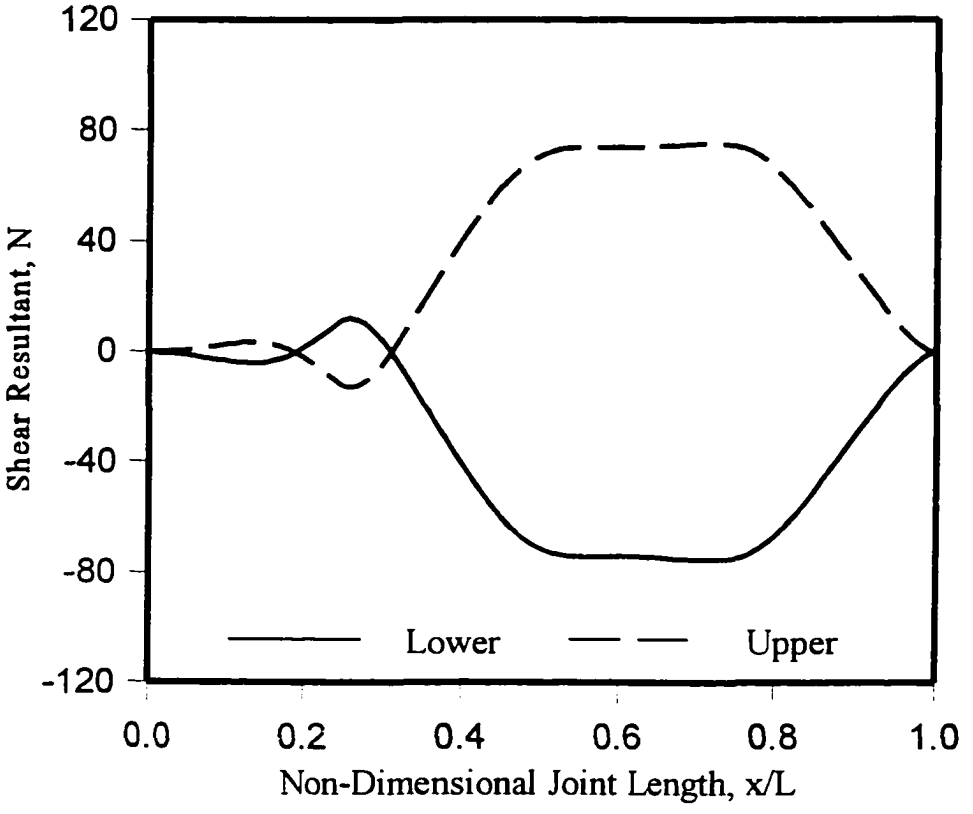

Figure 32 Shear Stress Resultant - Crossply

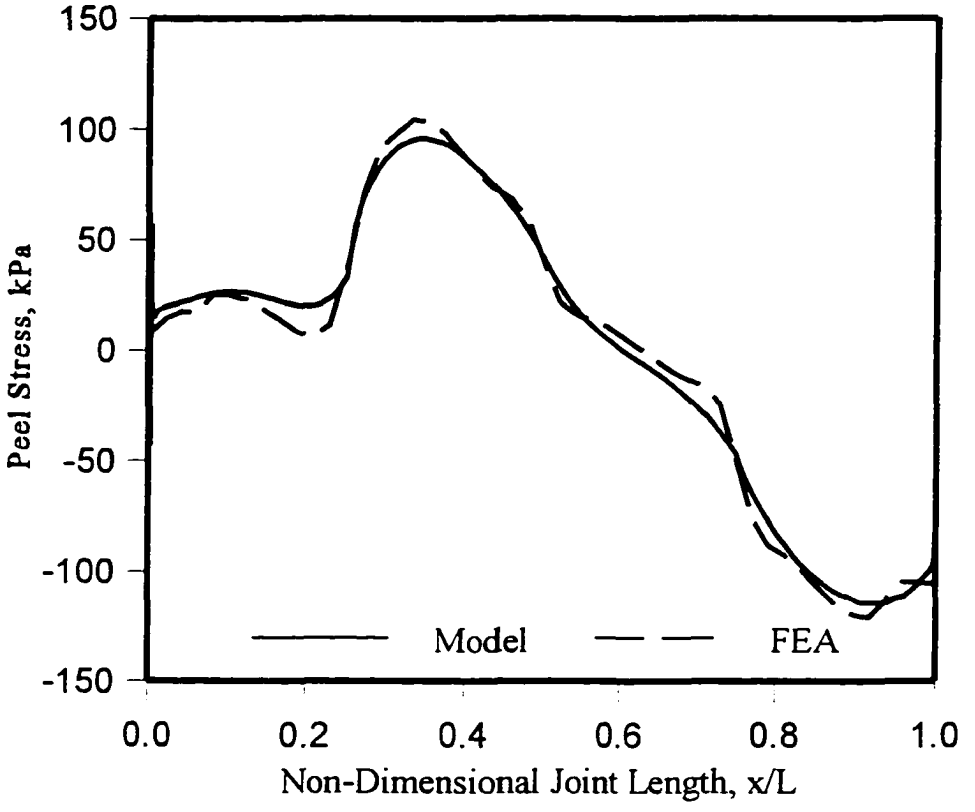

Figure 33 Adhesive Peel Stress - Crossply

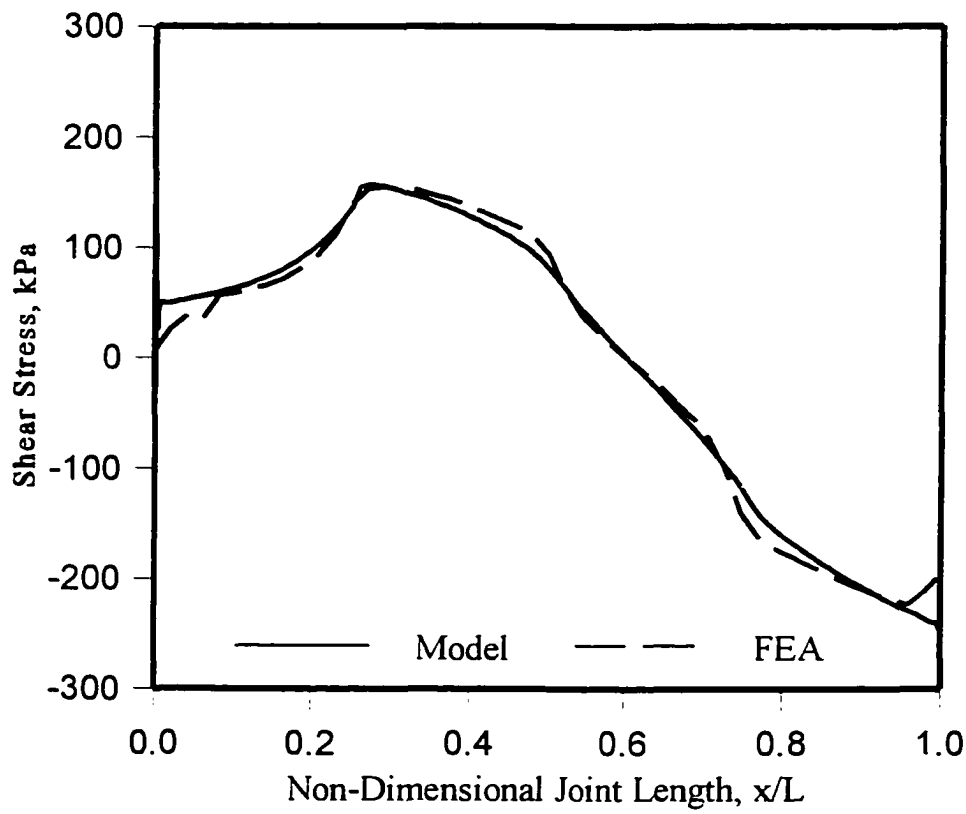

Figure 34 Adhesive Shear Stress - Crossply

CHAPTER 7

CONCLUSIONS

Two analytical models have been developed to describe the taper-taper adhesive-bonded joint under tension loading, a mechanics of materials model and a laminated plate model. The laminated plate model was also solved for the case of four-point bending.

The mechanics of materials model was based on the assumption of an isotropic adhesive and used the extensional Young's modulus to characterize the plates. The laminates were assumed to be in the plane strain condition under a tension load. Using this model the strain distribution in the laminates was obtained through numerical integration of the set of eight simultaneous first-order, linear ordinary differential equations with variable coefficients. A FORTRAN program was developed to carry out the integration. The model appeared to be reasonably accurate in the area of the joint that was modeled and could be used for joint design after suitable refinement and experimental testing to prove its accuracy.

The laminated plate model was developed to overcome some of the limitations of the mechanics of materials model. The analytical model of the strain-stress distributions in an adhesive-bonded taper-taper joint under tension loading was developed for unidirectional and crossply laminates using classical laminated plate theory. Shear correction factors were used to account for transverse shear deformation. The developed model consists of eighteen simultaneous, linear, first-order differential equations with variable coefficients. A FORTRAN program was developed to implement the Linear Shooting Method to numerically integrate the model. The program was developed and run on an IBM

compatible personal computer. The analytical model compares well with the finite element models and computes the peak adhesive peel and shear stresses to within about 5 - 8 % of those predicted by finite element analysis. The model can be used to analyze joints for safe, efficient design.

A laminated plate model was also derived for the case of cylindrical bending. The model consisted of six, simultaneous, second-order differential equations. The FORTRAN program used to solve the tension model was modified to solve this case. The model results agreed well with the finite element model. The adhesive stresses predicted were within about 2% of the finite element results. The model can be used to analyze joints for safe, efficient design.

Further study of this joint is warranted. The preliminary buckling analysis in Appendices A and B will be completed in the future.

REFERENCES

1. Kutscha, D., 1964, "Mechanics of Adhesive-Bonded Lap-Type Joints: Survey and Review," Technical Report AFML-TDR-64-298.

2. Kutscha, D., and Hofer, K.E. Jr., 1969, "Feasibility of Joining Advanced Composite Flight Vehicles," Technical Report AFML-TR-68-391.

3. Matthews, F.L., Kilty, P.F., and Goodwin, E.W., 1982, "A Review of the Strength of Joints in Fibre-Reinforced Plastics: Part 2 Adhesively Bonded Joints," *Composites*, pp. 29-37.

4. Vinson, J.R., 1989, "Adhesive Bonding of Polymer Composites," *Polymer Engineering and Science*, Vol. 29, No. 19, pp. 1325-1331.

5. Hart-Smith, L.J., 1974, "Analysis and Design of Advanced Composite Bonded Joints" Douglas Aircraft Co., NASA Contract Report CR-2218.

6. Adams, R.D. and W.C. Wake, 1984, *Structural Adhesive Joints in Engineering*, Elsevier Applied Science Publishers, London & New York.

7. Baluch, M.H., G.Z. Voyiadjis and A.K. Azad, 1984, "A Refined Theory for Isotropic Plates," *Transactions, Canadian Society for Mechanical Engineering*, Vol. 8, No. 1, pp. 21-27.

8. Voyiadjis, G.Z., Baluch,M.H., and Chi, W.K., 1985, "Effects of Shear and Normal Strain on Plate Bending," *Journal of Engineering Mechanics*, Vol. 111, pp. 1130-1143.

9. Reissner, E., 1975, "On Transverse Bending of Plates, Including the Effect of Transverse Shear Deformation," *Journal of Solids Structures*, Vol. 11, No. 5-D, pp. 569-573.

10. Whitney, J.M., 1969, "The Effect of Transverse Shear Deformation on the Bending of Laminated Plates," *Journal of Composite Materials*, 3(3), pp. 534-547.

11. Whitney, J.M., and N.J. Pagano, 1970, "Shear Deformation in Heterogenous Anisotropic Plates," *Journal of Applied Mechanics*, Vol. 37, pp. 1031-1036.

12. Whitney, J.M., 1972, "Stress Analysis of Thick Laminated Composite and Sandwich Plates," *Journal of Composite Materials*, Vol. 6, pp. 426-440.

13. Khdeir, A.A., J.N. Reddy, and L. Librescu, 1987, "Analytical solution of a Refined Shear Deformation Theory for Rectangular Composite Plates," *International Journal of Solids Structures*, Vol. 23, No. 10, pp. 1447-1463.

14. Whitney, J.M., and A.W. Leissa, 1969, "Analysis of Heterogenous Anisotropic Plates," *Journal of Applied Mechanics*, Vol. 36, pp. 261-266.

15. Lo, K.H., R.M. Christensen, and E.M. Wu, 1977, "A Higher-Order Theory of Plate Deformation, Part 1: Homogenous Plates," *Journal of Applied Mechanics*, Vol. 44, pp. 663-668.

16. Lo, K.H., R.M. Christensen, and E.M. Wu, 1977, "A Higher-Order Theory of Plate Deformation, Part 2: Laminated Plates," *Journal of Applied Mechanics*, Vol. 44, pp. 669-676.

17. Medwadowski, S.J., 1958, "A Refined Theory for Elastic Orthotropic Plates," *Journal of Applied Mechanics*, Vol. 25, pp. 437-443.

18. Whitney, J.M., 1969, "Bending-Extensional Coupling in Laminated Plates Under Transverse Loading," *Journal of Composite Materials*, Vol. 3, pp. 20-28.

19. Pagano, N.J., 1969, "Exact Solutions for Composite Laminates in Cylindrical Bending," *Journal of Composite Materials*, Vol. 3, pp. 398-411.

20. Whitney, J.M., 1969 "Cylindrical Bending of Unsymmetrically Laminated Plates," *Journal of Composite Materials*, Vol. 3, pp. 715-719.

21. Pagano, N.J. 1970, "Influence of Shear Coupling in Cylindrical Bending of Anisotropic Laminates," *Journal of Composite Materials*, Vol. 4, pp. 330-343.

22. Toledano, A., and H. Murakami, 1987, "A High-Order Laminated Plate Theory with Improved In-Plane Responses," *International Journal of Solids Structures*, Vol. 23, No. 1, pp. 111-131.

23. Pandya, B.N., and T. Kant, 1988, "Higher-Order Shear Deformable Theories for Flexure of sandwich Plates - Finite Element Evaluations," *International Journal of Solids Structures*, Vol. 24, No. 12, pp. 1267-1286.

24. Reddy, J.N., 1984, "A Simple Higher-Order Theory for Laminated Plates," *Journal of Applied Mechanics*, Vol. 51, pp. 745-752.

25. Spilker, R.L., and S.C. Chou, 1980, "Edge Effects in Symmetric Composite Laminates: Importance of Satisfying the Traction-Free-Edge Condition," *Journal of Composite Materials*, Vol. 14, No. 1, p. 2.

26. Pagano, N.J., 1970, "Exact Solutions for Rectangular Bidirectional Composites and Sandwich Plates," *Journal of Composite Materials*, Vol. 4, pp. 20-35.

27. Pipes, R.B. and Pagano, N.J., 1970, "Interlaminar Stresses in Composite Laminates Under Uniform Axial Extension," *Journal of Composite Materials*, Vol. 4., pp. 538-548.

28. Chou, P.C. and Carleone, J., 1973, "Transverse Shear in Laminated Plate Theories," *AIAA Journal*, Vol. 11, No. 9, pp. 1333-1336.

29, Whitney, J.M., 1972, "Shear Correction Factors for Orthrotropic Laminates Under Static Loading," *Journal of Composite Materials*, Vol. 6, pp. 426-440.

30. Goland, M., and Reissner, E., 1944, "The Stresses in Cemented Joints," *Journal of Applied Mechanics*, pp. A-17,A-27.

31. Hart-Smith, L.J., 1973a, "Adhesive-Bonded Single-Lap Joints," Douglas Aircraft Co., NASA Contract Report CR-112236.

32. Hart-Smith, L.J., 1973b, "Adhesive-Bonded Double-Lap Joints," Douglas Aircraft Co., NASA Contract Report CR-112235.

33. Reissner, E., 1945, "The Effect of Transverse Shear Deformation on the Bending of Elastic Plates," *Journal of Applied Mechanics*," No. 12, pp. A-69-A-77.

34. Reddy, J.N., 1984, A Refined Nonlinear Theory of Plates with Transverse Shear Deformation," *International Journal of Solids Structures*, Vol. 20, No. 9/10, pp. 881-896.

35. Sharpe, W.N., Jr. and T.J. Muha, Jr., 1974, Comparison of Theoretical and Experimental Shear Stress in the Adhesive Layer of a Lap Bonded Joint Model," *AMMRC MS 74-8*.

36. McLaren, A.S. and I. MacInnes, 1958, "The Influence on the Stress Distribution in an Adhesive Lap Joint of Bending of the Adhering Sheets," *Brit. J. of Appl. Phys.*, 9, p. 72.

37. Wah, T., 1973, "Stress Distribution in a Bonded Anisotropic Lap Joint," *Journal Engineering Materials and Technology*, Vol. 95, No. 3, p. 174.

38. Allred, R.E., and T.R. Guess, 1978, "Efficiency of Double-Lapped Composite Joints in Bending," *Composites*, 9, No. 24, p. 112.

39. Cheng, S., Du Chen and Shi Yupu, 1991, "Analysis of Adhesive-Bonded Joints with Nonidentical Adherends," *Journal of Engineering Mechanics*, Vol. 117, No. 3, pp 605-623.

40. Delale, F., F. Erdogan and M.N. Aydinoglu, 1981, "Stresses in Adhesively Bonded Joints: A Closed-Form Solution," *J. Composite Materials*, Vol. 15, p. 249.

41. Renton, W.J., 1976, "The Symmetric Lap-Shear Test - What Good Is It?," *Experimental Mechanics*, p. 409.

42. Griffin, S.A., Pang, S.S., and Yang, C., 1991, "Strength Model of Adhesive Bonded Composite Pipe Joints Under Tension," *Polymer Engineering and Science*, Vol. 31, No.7, pp. 533-538.

43. Yang, C., and Pang, S.S., 1996, "Stress-Strain Analysis of Single-Lap Composite Joints Under Tension," *Journal Engineering Materials and Technology*, Vol. 118, pp. 247-255.

44. Hart-Smith, L.J., 1973c, "Adhesive-Bonded Scarf And Stepped-Lap Joints," Douglas Aircraft Co., NASA Contract Report CR-112237.

45. Wah, T., 1976, "The Adhesive Scarf Joint in Pure Bending," *Int. Journal Mechanical Science, Vol. 18*, pp 223-228.

46. Sage, C.N., 1978, "Pure Shear Fatigue of an Adhesive with Reference to Unidirectional Composite Bonded Joints," *Symposium Jointing in Fibre Reinforced Plastics*, Imperial College, London (IPC Press).

47. Erdogan, F., and M. Ratwani, 1978, "Stress Distribution in Bonded Joints," *Journal of Composite Materials*, Vol. 5, pp 378-393.

48. Helms, J.E., Yang, C., and Pang, S.S., 1996, "Strain Distribution in a Taper-Taper Adhesive-Bonded Joint in Composite Flat Plates," *Journal of Thermoplastic Composite Materials*, Vol. 9, No. 3, pp. 280-291.

49. Helms, J.E., Yang, C., and Pang, S.S., 1997, "A Laminated Plate Model of an Adhesive-Bonded Taper-Taper Joint Under Tension," *Journal of Engineering Materials and Technology*, Vol. 119, pp. 408-414.

61. Sanchez, D.A., 1968, *Ordinary Differential Equations and Stability Theory: An Introduction*, W.H. Freeman and Company.

62. Burden, R.L., and J.D. Faires, 1985, *Numerical Analysis*, Weber and Schmidt.

63. Whitney, J.M., 1987, *Structural Analysis of Laminated Anisotropic Plates*, Technomic Publishing Company, Inc.

64. Mindlin, R.D., 1951, "Influence of Rotary Inertia and Shear on Flexural Motions of Isotropic, Elastic Plates," *Journal of Applied Mechanics*, Vol. 18, pp. 336-343.

65. Press, W.H., Teukolsky, S.A., Vetterling, W.T., and Flannery, B.P., 1994, *Numerical Recipes in FORTRAN*, Second Edition, Cambridge University Press.

66. Keller, H.B., 1992, *Numerical Methods For Two-Point Boundary Problems*, Dover Publishing, New York.

67. COSMOS/M Finite Element System User Guide, Version 1.65A, 1992, Structural Research And Analysis Corporation.

68. Tsai, S.W. and Hahn, H.T., 1990, *Introduction to Composite Materials*, Technomic Publishing, Lancaster, PA.

69. Timoshenko, S.P., 1961, *Theory of Elastic Stability*, McGraw-Hill Publishing Co.

APPENDIX A

BUCKLING ANALYSIS

To complete the study of the taper-taper adhesive-bonded joint the behavior of the joint under compressive loading should be studied. The following development outlines buckling analysis of the joint. First-order laminated plate theory was used in the derivation of this model. Shear correction factors were included to account for transverse shear deformation. Three steps were followed in the derivation of the analytical model. A description of each step is detailed below.

(a) Kinematical Relations

Figure A1 is a drawing of the taper-taper joint under a compressive in-plane load.

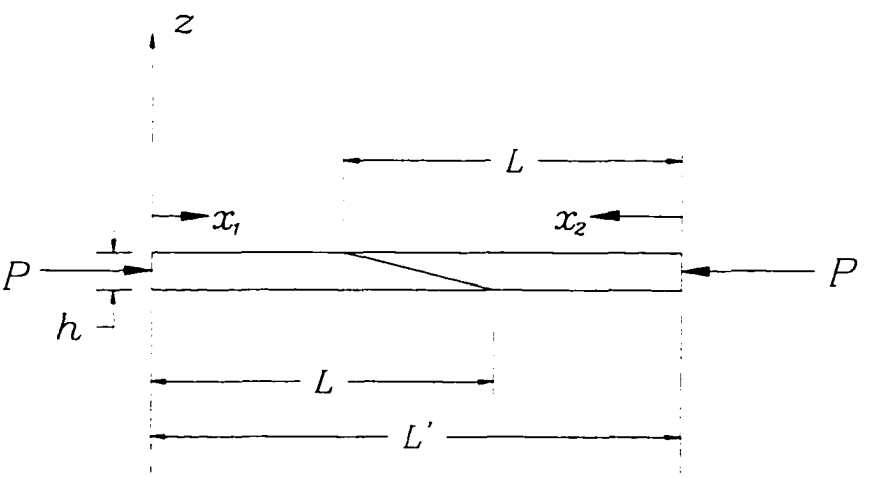

Figure A1 Joint with Compression Loading

A standard right hand x, y, z coordinate system was used in the derivation of the model as shown in Fig. A2. The x and y coordinates are defined in the mid-plane of the laminate.

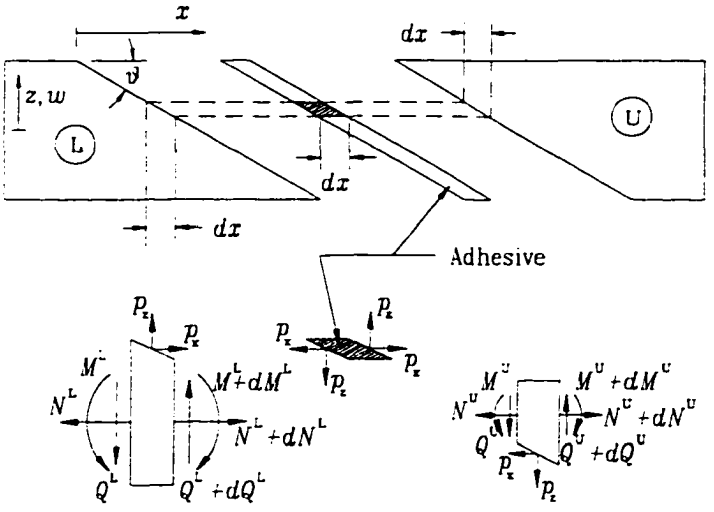

Figure A2 Freebody Diagram of the Joint - Compression Loading

The tangential displacement in the x-direction was assumed to be a linear function of the through laminate coordinate, that is

$$u = u^{o}(x) + z\,\psi_x(x)$$
$$w = w(x) \tag{A1}$$

where u^o is the tangential displacement of the mid-plane in the x-direction, ψ_x is the corresponding bending slope, and w is the deflection in the z-direction. The transverse strain is

$$\epsilon_{zz} = \psi_x(x) + \frac{dw}{dx} \tag{A2}$$

The strain-displacement relation is

$$\epsilon_x = \epsilon_x^o + z\,\kappa_x \tag{A3}$$

where the mid-plane strain and x-direction curvature can be represented as shown in Eq. (A4):

$$\epsilon_x^o = \frac{du^o}{dx} \quad ; \quad \kappa_x = \frac{d\psi_x}{dx} \tag{A4}$$

(b) Energy Formulation

The total strain energy for the orthotropic plates and adhesive can be written as

$$U = \frac{1}{2}\iiint_V (Q_{11}^{(i)}\,\epsilon_x^2 + k\,Q_{55}^{(i)}\epsilon_{xz}^2 + 2\,E_{adhesive})\,dxdydz \tag{A5}$$

where k is the shear correction factor, $Q_{11}^{(i)}$ is the ith ply stiffness and $Q_{55}^{(i)}$ is the shear stiffness of the ith ply and

$$E_{adhesive} = \frac{1}{2}[\lambda e^2 + 2G\,(\epsilon_x^2 + \epsilon_z^2) + G\,\epsilon_{xz}^2]$$
$$and \quad e = \epsilon_x + \epsilon_z \quad and \quad \lambda = \frac{\nu E}{(1+\nu)(1-2\nu)} \tag{A6}$$

where E and G are the modulus of elasticity and shear modulus of the adhesive and ν is Poisson's ratio for the adhesive.

The potential energy of in-plane loads is

$$V = \iint N_x'\epsilon_x'\,dxdy \tag{A7}$$

where N_x' is the initial in-plane force applied to the plate in a pre-buckled state and ϵ_x' is the mid-plane strain due to the large deflection w in the z direction, that is,

$$\epsilon_x' = \frac{du^o}{dx} + \frac{1}{2}\left(\frac{dw}{dx}\right)^2 \tag{A8}$$

Substituting into the expression for potential energy

$$V = \iint N_x' \left[\frac{du^o}{dx} + \frac{1}{2}\left(\frac{dw}{dx} \right)^2 \right] dxdy \qquad \text{(A9)}$$

For the case in question

$$N_x' = -P \qquad \text{(A10)}$$

Since there is an absence of transverse loading the work due to transverse loading is

$$W = 0 \qquad \text{(A11)}$$

(c) Ritz Method

The Ritz Method is a convenient method for obtaining approximate solutions to boundary value problems [63]. The problem can be formulated by setting the first variation of the total energy to zero,

$$\delta\Pi = \delta\ (U + V + W) = 0 \qquad \text{(A12)}$$

To derive a solution known functions are chosen for each of the variables. For this study Fourier Series were chosen to represent all of the displacement variables. The geometric boundary conditions must be satisfied by these series. Also the series must be continuous through at least the same order derivatives as required in the corresponding differential equations.

To facilitate the analysis the assembly was divided into two regions as shown in Fig. A1. Eqs. (A5) and (A6) are written for each region and then combined into Eq. (A12). Fourier series were chosen to meet the boundary conditions at each end of the assembly.

The boundary conditions are

$$w = 0 \; at \; x = 0 \; \& \; x = L$$

$$\frac{dw}{dx} = 0 \; at \; x = 0 \; \& \; x = L \tag{A13}$$

$$u_2^o = 0 \; at \; x = L'$$

In section one the following Fourier series were chosen

$$u_1^o = u_0 - \frac{u_0 \, x_1}{L'} + \sum_{i=1}^{\infty} A_i \sin \frac{i \, \pi \, x_1}{L}$$

$$\psi_1 = \sum_{k=1}^{\infty} B_k \sin \frac{k \, \pi \, x_1}{2 \, L} \tag{A14}$$

$$w_1 = \sum_{m=1}^{\infty} C_m \left(1 - \cos \frac{m \, \pi \, x_1}{L} \right)$$

where L is the length of each laminate, L' is the length of the assembly and u_o is the static deflection of the assembly.

In section 2 the following series were chosen

$$u_2^o = \frac{u_0 \, x_2}{L'} + \sum_{i=1}^{\infty} D_i \sin \frac{i \, \pi \, x_2}{L}$$

$$\psi_2 = \sum_{k=1}^{\infty} E_k \sin \frac{k \, \pi \, x_2}{2 \, L} \tag{A15}$$

$$w_2 = \sum_{m=1}^{\infty} F_m \left(1 - \cos \frac{m \, \pi \, x_2}{L} \right)$$

The adhesive stresses σ_x, σ_y and τ_{xy} can be related to the adhesive mechanical properties and the laminate displacement fields as

$$\sigma_x = E\frac{\partial u}{\partial x} = \frac{E\,(u^U - u^L)}{s}$$

$$\sigma_z = E\frac{\partial w}{\partial z} = \frac{E(w^U - s\left(\frac{dw^U}{dx}\right) - w^L)}{s\tan\theta} \qquad \text{(A16)}$$

$$\tau_{xz} = G\left(\frac{\partial u}{\partial z} + \frac{\partial w}{\partial x}\right) = G\left(\frac{u^U - s\left(\frac{\partial u^U}{\partial x}\right) - u^L}{s\tan\theta} + \frac{w^U - w^L}{s}\right)$$

where E and G are the Young's and shear moduli of the adhesive, s is the horizontal distance across the adhesive in the x-direction, and the displacement variables, u and w, are defined in Eq. (A1).

When the series above (Eqs. (A14)-(A15)) and the adhesive relations, Eq. (A16) are substituted into the expression for Π, the first variation is taken and the resulting integrals are evaluated considering the orthogonality of the series, a general eigenvalue problem is obtained. The resulting equations can be expressed in matrix form as

$$\left(\left[K_f\right] - P\left[K_g\right]\right)\{X_i\} = 0 \qquad \text{(A17)}$$

where K_f is the stiffness matrix, K_g is the incremental geometric stiffness matrix, P is the applied load and the X_i are the undetermined coefficients of the assumed Fourier series. Equation (A17) can be re-arranged to yield

$$\left(\left[K_g\right] - \frac{1}{P}\left[K_f\right]\right)\{X_i\} = \left(\left[K_g\right] - \lambda\left[K_f\right]\right)\{X_i\} = 0 \qquad \text{(A18)}$$

And finally a standard eigenvalue problem is obtained:

$$\left[[K_f]^{-1}[K_g] - \lambda[I] \right]\{X_i\} = 0 \qquad \text{(A19)}$$

where $[I]$ is the identity matrix. To solve this problem, the determinant of the equation in brackets is set equal to zero. The largest eigenvalue, λ_{max}, was calculated and $P = 1/\lambda_{max}$ yielded the desired critical buckling load.

The stiffness matrix, K_f, is necessarily symmetric, therefore, only elements along and to the right of the major diagonal are shown in the equations listed in Appendix B. The symbols, such as IN22, are integrals that must be evaluated numerically. The integrals are defined below the equations. A prime on an integral, i.e., IN22', indicates that the integral should be evaluated with the i and j indexes interchanged.

A personal computer program will be developed in FORTRAN to solve Eq. (A19).

APPENDIX B

ELEMENTS OF THE STIFFNESS MATRIX

$$
\begin{aligned}
\frac{\partial \Pi}{\partial u_o} = \sum & \left[\begin{array}{l} \frac{IN1+IN10}{L'^2} + 4\left(\frac{E}{s^2 L'^2} + \frac{G}{s^2 \tan^2\theta L'}\right) IN47 \\ -4\left(\frac{E}{s^2 L'^2} + \frac{G}{sL'^2 \tan^2\theta} + \frac{G}{s^2 \tan^2\theta L'}\right) IN46 \\ +\left(\frac{E}{s^2} + \frac{G}{\tan^2\theta L'^2} + \frac{G}{2stan^2\theta L'} + \frac{G}{s^2 \tan^2\theta}\right) IN48 \end{array} \right] u_o \\
& + \sum \left[\frac{-j\pi IN2}{LL'} - 2\left(\frac{E}{s^2 L'} + \frac{G}{s^2 \tan^2\theta L'}\right) IN19 + \left(\frac{E}{s^2} + \frac{G}{stan^2 L'} + \frac{G}{s^2 \tan^2\theta}\right) IN31 \right] A_j \\
& + \sum \left[\frac{-j\pi IN4}{2LL'} - 2\left(\frac{E}{2s^2 L'} + \frac{G}{s^2 \tan^2\theta L'}\right) IN30' + \left(\frac{E}{s^2} + \frac{G}{stan^2\theta L'} + \frac{G}{s^2 \tan^2\theta}\right) IN20 \right] B_j \\
& + \sum \left[\begin{array}{l} -2\left(\frac{G+\nu E}{s^2 \tan\theta L'}\right) IN46 + 2\left(\frac{G+\nu E}{s^2 \tan\theta L'}\right) IN29 + \left(\frac{G}{stan\theta L'} + \frac{G+\nu E}{s^2 \tan\theta}\right) IN48 \\ -\left(\frac{G}{stan\theta L'} + \frac{G+\nu E}{s^2 \tan\theta}\right) IN33' \end{array} \right] C_j \\
& + \sum \left[\begin{array}{l} \frac{j\pi IN11}{LL'} + 2\left(\frac{E}{s^2 L'} + \frac{G}{s^2 \tan^2\theta L'}\right) IN19 - \left(\frac{E}{s^2} + \frac{G}{stan^2\theta L'} + \frac{G}{s^2 \tan^2\theta}\right) IN31 \\ -\frac{2Gj\pi IN29}{stan^2\theta LL'} + Gj\pi\left(\frac{1}{\tan^2\theta LL'} + \frac{1}{stan^2\theta L'}\right) IN33' \end{array} \right] D_j \\
& + \sum \left[\begin{array}{l} \frac{j\pi IN13}{2LL'} + 2\left(\frac{E}{s^2 L'} + \frac{G}{s^2 \tan^2\theta L'}\right) IN23 + \left(\frac{E}{s^2} + \frac{G}{s^2 \tan^2\theta} + \frac{G}{stan^2\theta L'}\right) IN22 \\ -\frac{Gj\pi}{2}\left(\frac{1}{stan^2\theta LL'} + \frac{1}{s^2 \tan^2\theta L}\right) IN37 + \frac{3Gj\pi IN40}{4s^2 \tan^2\theta LL'} + \frac{GIN51}{s^2 \tan^2\theta L'} \\ -\frac{G}{2}\left(\frac{1}{stan\theta L'} + \frac{1}{s^2 \tan\theta}\right) IN44 \end{array} \right] E_j \\
& + \sum \left[\begin{array}{l} 2\left(\frac{G+\nu E}{s^2 \tan\theta L'}\right) IN46 - 2\left(\frac{G+\nu E}{s^2 \tan\theta L'}\right) IN29 - \left(\frac{G}{stan\theta L'} + \frac{G+\nu E}{s^2 \tan\theta}\right) IN48 \\ +\left(\frac{G}{stan\theta L'} + \frac{G+\nu E}{s^2 \tan\theta}\right) IN33' - \frac{3\nu Ej\pi IN19}{stan\theta LL'} + \frac{\nu Ej\pi IN31}{stan\theta L'} \end{array} \right] F_j
\end{aligned}
\tag{B1}
$$

$$\frac{\partial \Pi}{\partial A_i} = \sum \left[\frac{ij\pi^2 IN3}{L^2} + \left(\frac{E}{s^2} + \frac{G}{s^2 \tan^2\theta}\right) IN32 \right] A_j$$
$$+ \sum \left[\frac{ij\pi^2 IN5}{2L^2} + \frac{EIN21}{2s^2} + \left(\frac{E}{2s^2} + \frac{G}{s^2 \tan^2\theta}\right) IN26' \right] B_j$$
$$+ \sum \left[\left(\frac{G+\nu E}{s^2 \tan\theta}\right) IN31' - \left(\frac{G+\nu E}{s^2 \tan\theta}\right) IN35' \right] C_j$$
$$+ \sum \left[-\left(\frac{E}{s^2} + \frac{G}{2s^2\tan^2\theta}\right) IN32 - \frac{GIN35}{2s^2\tan^2\theta} + \frac{Gj\pi IN35'}{s \tan^2\theta L} \right] D_j$$
$$+ \sum \left[\left(\frac{E}{s^2} + \frac{G}{s^2 \tan^2\theta}\right) IN24 - \frac{Gj\pi IN43'}{2s^2\tan^2\theta L} - \frac{GIN49}{2s^2\tan\theta} \right] E_j$$
$$+ \sum \left[-\left(\frac{G+\nu E}{s^2 \tan\theta}\right) IN31' + \left(\frac{G+\nu E}{s^2 \tan\theta}\right) IN35' + \frac{\nu Ej\pi IN32}{s\tan\theta L} \right] F_j \qquad \text{(B2)}$$

$$\frac{\partial \Pi}{\partial B_i} = \sum \left[\frac{ij\pi^2 IN6}{4L^2} + k^L IN7 + \left(\frac{E}{s^2} + \frac{G}{s^2\tan^2\theta}\right) IN25 \right] B_j$$
$$+ \sum \left[\frac{k^L j\pi IN8}{L} + \left(\frac{G+\nu E}{s^2\tan\theta}\right) IN20' - \left(\frac{G+\nu E}{s^2\tan\theta}\right) IN39' \right] C_j$$
$$+ \sum \left[-\left(\frac{E}{s^2} + \frac{G}{s^2\tan^2\theta}\right) IN26 - \frac{GIN21'}{s^2\tan^2\theta} - \frac{Gj\pi IN39'}{s\tan^2\theta L} \right] D_j$$
$$+ \sum \left[\left(\frac{E}{s^2} + \frac{G}{2s^2\tan^2\theta}\right) IN27 + \frac{GIN27'}{2s^2\tan^2\theta} + \frac{Gj\pi IN45}{2s^2\tan^2\theta L} - \frac{GIN54'}{4s^2\tan\theta} - \frac{GIN54}{4s^2\tan\theta} \right] E_j$$
$$+ \sum \left[-\left(\frac{G+\nu E}{s^2\tan\theta}\right) IN20' + \left(\frac{G+\nu E}{s^2\tan\theta}\right) IN39' + \frac{\nu Ej\pi IN26}{s \tan\theta\ L} \right] F_j \qquad \text{(B3)}$$

$$\frac{\partial \Pi}{\partial C_i}=\sum\left[\begin{array}{c}\frac{-Pi^2\pi^2}{2L}+\frac{k^{L}ij\pi^2IN9}{L^2}+(\frac{E}{s^2\tan^2\theta}+\frac{G}{s^2})IN48\\ +(\frac{2E}{s^2\tan^2\theta}+\frac{G}{s^2})IN33'+(\frac{E}{s^2\tan^2\theta}+\frac{G}{s^2})IN34-\frac{GIN33}{s^2}\end{array}\right]C_j$$
$$+\sum\left[-(\frac{G+\nu E}{s^2\tan\theta})IN31+(\frac{G+\nu E}{s^2\tan\theta})IN35+\frac{Gj\pi IN33'}{s\tan\theta L}-\frac{Gj\pi IN34'}{s\tan\theta L}\right]D_j$$
$$+\sum\left[\begin{array}{c}\frac{G+\nu E}{s^2\tan\theta})IN22-\frac{G+\nu E}{s^2\tan\theta})IN36'-\frac{Gj\pi IN37}{2s^2\tan\theta L}\\ +\frac{Gj\pi IN38}{2s^2\tan\theta L}-\frac{GIN44}{2s^2}+\frac{GIN55}{2s^2}\end{array}\right]E_j$$
$$+\sum\left[\begin{array}{c}-(\frac{E}{s^2\tan^2\theta}+\frac{G}{s^2})IN48+(\frac{E}{s^2\tan^2\theta}+\frac{G}{s^2})IN33+(\frac{E}{s^2\tan^2\theta}+\frac{G}{s^2})IN33'\\ +\frac{Ej\pi IN31}{s\tan^2\theta L}-\frac{Ej\pi IN35}{s\tan^2\theta L}-(\frac{E}{s^2\tan^2\theta}+\frac{G}{s^2})IN34\end{array}\right]F_j \qquad \text{(B4)}$$

$$\frac{\partial \Pi}{\partial D_i}=\sum\left[\begin{array}{c}\frac{ij\pi^2IN12}{L^2}+(\frac{E}{s^2}+\frac{G}{s^2\tan^2\theta})IN32-\frac{Gj\pi IN35'}{s\tan^2\theta L}\\ -\frac{Gj\pi IN35}{s\tan^2\theta L}+\frac{Gj\pi IN43'}{2s^2\tan^2\theta L}+\frac{Gij\pi^2IN34}{\tan^2\theta L^2}\end{array}\right]D_j$$
$$+\sum\left[\begin{array}{c}\frac{ij\pi^2IN14}{2L^2}-(\frac{E}{s^2}+\frac{G}{s^2\tan^2\theta}+\frac{Gi\pi}{2s\tan^2\theta L})IN24+\frac{Gi\pi IN36'}{2s\tan^2\theta L}\\ -\frac{G}{4}(\frac{j\pi}{s\tan^2\theta L}+\frac{ij\pi^2}{s\tan^2\theta L^2})IN38+\frac{Gj\pi IN43'}{4s^2\tan^2\theta L}+\frac{GIN49}{2s^2\tan\theta}-\frac{Gi\pi IN55}{2s\tan\theta L}\end{array}\right]E_j$$
$$+\sum\left[(\frac{G+\nu E}{s^2\tan\theta})IN31'-\frac{Gi\pi IN33}{s\ \tan\theta\ L}+\frac{Gi\pi IN34}{s\tan\theta L}-(\frac{G+\nu E}{s^2\tan\theta})IN35'-\frac{\nu Ej\pi IN32}{s\tan\theta L}\right]F_j \qquad \text{(B5)}$$

$$\frac{\partial \Pi}{\partial E_i}=\sum\left[\begin{array}{c}\frac{ij\pi^2 IN15}{4L^2}+k^U IN16+(\frac{E}{s^2}+\frac{G}{s^2\tan^2\theta})IN28-\frac{Gj\pi IN41'}{2s^2\tan^2\theta L}-\frac{Gij\pi^2 IN41}{2s^2\tan^2\theta L} \\ +\frac{Gij\pi^2 IN42}{4s^2\tan^2\theta L^2}-\frac{GIN50}{s^2\tan\theta}+\frac{Gj\pi IN52'}{4s^2\tan\theta L}+\frac{Gi\pi IN52}{4s^2\tan\theta L}-\frac{GIN53}{4s^2}\end{array}\right]E_j$$
$$+\sum\left[\begin{array}{c}\frac{k^U j\pi IN17}{L}-(\frac{G+\nu E}{s^2\tan\theta})IN22'+(\frac{G+\nu E}{s^2\tan\theta})IN36+\frac{Gi\pi IN37'}{2s^2\tan\theta L} \\ -\frac{Gi\pi IN38'}{2s^2\tan\theta L}+\frac{\nu Ej\pi IN24'}{s\tan\theta L}+\frac{GIN44'}{2s^2}-\frac{GIN55'}{2s^2}\end{array}\right]F_j \quad \text{(B6)}$$

$$\frac{\partial \Pi}{\partial F_i}=\sum\left[\begin{array}{c}\frac{-Pi^2\pi^2}{2L}+\frac{k^U ij\pi^2 IN18}{L^2}+(\frac{E}{s^2\tan^2\theta}\frac{G}{s^2})IN48-(\frac{2E}{s^2\tan^2\theta}+\frac{G}{s^2})IN33 \\ +(\frac{E}{s^2\tan^2\theta}+\frac{G}{s^2})IN34-\frac{Ej\pi IN31}{s^2\tan^2\theta L}-\frac{Ej\pi IN35}{s\tan^2\theta L}-\frac{Ei\pi IN31'}{s\tan^2\theta L} \\ +\frac{Ei\pi IN35'}{s\tan^2\theta L}+\frac{Eij\pi^2 IN32}{\tan^2\theta L^2}-\frac{GIN33}{s^2}\end{array}\right]F_j \quad \text{(B7)}$$

$$IN1=\int_0^L A_{11}^L dx \quad \text{(B8)}$$

$$IN2=\int_0^L A_{11}^L \cos\frac{j\pi x}{L}dx \quad \text{(B9)}$$

$$IN3=\int_0^L A_{11}^L \cos\frac{i\pi x}{L}\cos\frac{j\pi x}{L}dx \quad \text{(B10)}$$

$$IN4=\int_0^L B_{11}^L \cos\frac{j\pi x}{2L}dx \tag{B11}$$

$$IN5=\int_0^L B_{11}^L \cos\frac{i\pi x}{L}\cos\frac{j\pi x}{2L}dx \tag{B12}$$

$$IN6=\int_0^L D_{11}^L \cos\frac{i\pi x}{2L}\cos\frac{j\pi x}{2L}dx \tag{B13}$$

$$IN7=\int_0^L A_{55}^L \sin\frac{i\pi x}{2L}\sin\frac{j\pi x}{2L}dx \tag{B14}$$

$$IN8=\int_0^L A_{55}^L \sin\frac{i\pi x}{2L}\sin\frac{j\pi x}{L}dx \tag{B15}$$

$$IN9=\int_0^L A_{55}^L \sin\frac{i\pi x}{L}\sin\frac{j\pi x}{L}dx \tag{B16}$$

$$IN10=\int_0^L A_{11}^U dx \tag{B17}$$

$$IN11=\int_0^L A_{11}^U \cos\frac{j\pi x}{L}dx \tag{B18}$$

$$IN12=\int_0^L A_{11}^U \cos\frac{i\pi x}{L}\cos\frac{j\pi x}{L}dx \tag{B19}$$

$$IN13=\int_0^L B_{11}^U \cos\frac{j\pi x}{2L}dx \tag{B20}$$

$$IN14=\int_0^L B_{11}^U \cos\frac{i\pi x}{L}\cos\frac{j\pi x}{2L}dx \tag{B21}$$

$$IN15=\int_0^L D_{11}^U \cos\frac{i\pi x}{2L}\cos\frac{j\pi x}{2L}dx \tag{B22}$$

$$IN16=\int_0^L A_{55}^U \sin\frac{i\pi x}{2L}\sin\frac{j\pi x}{2L}dx \tag{B23}$$

$$IN17=\int_0^L A_{55}^U \sin\frac{i\pi x}{2L}\sin\frac{j\pi x}{L}dx \tag{B24}$$

$$IN18=\int_0^L A_{55}^U \sin\frac{i\pi x}{L}\sin\frac{j\pi x}{L}dx \tag{B25}$$

$$IN19=\int_{L_1}^L h_T x \sin\frac{j\pi x}{L}dx \tag{B26}$$

$$IN20=\int_{L_1}^L h_T h^L \sin\frac{j\pi x}{2L}dx \tag{B27}$$

$$IN21=\int_{L_1}^L h_T h^L \sin\frac{i\pi x}{L}\sin\frac{j\pi x}{2L}dx \tag{B28}$$

$$IN22=\int_{L_1}^L h_T h^U \sin\frac{j\pi x}{2L}dx \tag{B29}$$

$$IN23=\int_{L_1}^L h_T h^U x \sin\frac{j\pi x}{2L}dx \tag{B30}$$

$$IN24=\int_{L_1}^L h_T h^U \sin\frac{i\pi x}{L}\sin\frac{j\pi x}{2L}dx \tag{B31}$$

$$IN25=\int_{L_1}^{L} h_T(h^L)^2 \sin\frac{i\pi x}{2L}\sin\frac{j\pi x}{2L}dx \tag{B32}$$

$$IN26=\int_{L_1}^{L} h_T h^L \sin\frac{i\pi x}{2L}\sin\frac{j\pi x}{L}dx \tag{B33}$$

$$IN27=\int_{L_1}^{L} h_T h^L h^U \sin\frac{i\pi x}{2L}\sin\frac{j\pi x}{2L}dx \tag{B34}$$

$$IN28=\int_{L_1}^{L} h_T(h^U)^2 \sin\frac{i\pi x}{2L}\sin\frac{j\pi x}{2L}dx \tag{B35}$$

$$IN29=\int_{L_1}^{L} h_T x\cos\frac{j\pi x}{L}dx \tag{B36}$$

$$IN30=\int_{L_1}^{L} h_T h^L x\sin\frac{i\pi x}{2L}dx \tag{B37}$$

$$IN31=\int_{L_1}^{L} h_T \sin\frac{j\pi x}{L}dx \tag{B38}$$

$$IN32=\int_{L_1}^{L} h_T \sin\frac{i\pi x}{L}\sin\frac{j\pi x}{L}dx \tag{B39}$$

$$IN33=\int_{L_1}^{L} h_T \cos\frac{i\pi x}{L}dx \tag{B40}$$

$$IN34=\int_{L_1}^{L} h_T \cos\frac{i\pi x}{L}\cos\frac{j\pi x}{L}dx \tag{B41}$$

$$IN35=\int_{L_1}^{L} h_T \cos\frac{i\pi x}{L}\sin\frac{j\pi x}{L}dx \tag{B42}$$

$$IN36=\int_{L_1}^{L} h_T h^{U} \sin\frac{i\pi x}{2L}\cos\frac{j\pi x}{L}dx \tag{B43}$$

$$IN37=\int_{L_1}^{L} h_T h^{U} \cos\frac{j\pi x}{2L}dx \tag{B44}$$

$$IN38=\int_{L_1}^{L} h_T h^{U} \cos\frac{i\pi x}{L}\cos\frac{j\pi x}{2L}dx \tag{B45}$$

$$IN39=\int_{L_1}^{L} h_T h^{U}\cos\frac{i\pi x}{L}\sin\frac{j\pi x}{2L}dx \tag{B46}$$

$$IN40=\int_{L_1}^{L} h_T h^{U}x\cos\frac{j\pi x}{2L}dx \tag{B47}$$

$$IN41=\int_{L_1}^{L} h_T (h^{U})^2\cos\frac{i\pi x}{2L}\sin\frac{j\pi x}{2L}dx \tag{B48}$$

$$IN42=\int_{L_1}^{L} h_T (h^{U})^2\cos\frac{i\pi x}{2L}\cos\frac{j\pi x}{2L}dx \tag{B49}$$

$$IN43=\int_{L_1}^{L} h_T h^{U}\cos\frac{i\pi x}{2L}\sin\frac{j\pi x}{L}dx \tag{B50}$$

$$IN44=\int_{L_1}^{L} h_T \sin\frac{j\pi x}{2L}dx \tag{B51}$$

$$IN45=\int_{L_1}^{L} h_T h^{L} h^{U}\sin\frac{i\pi x}{2L}\cos\frac{j\pi x}{2L}dx \tag{B52}$$

$$IN46=\int_{L_1}^{L} h_T x dx \tag{B53}$$

$$IN47=\int_{L_1}^{L} h_T x^2 dx \tag{B54}$$

$$IN48=\int_{L_1}^{L} h_T dx \tag{B55}$$

$$IN49=\int_{L_1}^{L} h_T \sin\frac{i\pi x}{L}\sin\frac{j\pi x}{2L} dx \tag{B56}$$

$$IN50=\int_{L_1}^{L} h_T h^U \sin\frac{i\pi x}{2L}\sin\frac{j\pi x}{2L} dx \tag{B57}$$

$$IN51=\int_{L_1}^{L} h_T x \sin\frac{j\pi x}{2L} dx \tag{B58}$$

$$IN52=\int_{L_1}^{L} h_T h^U \cos\frac{i\pi x}{2L}\sin\frac{j\pi x}{2L} dx \tag{B59}$$

$$IN53 = \int_{L_1}^{L} h_T \sin\frac{i\pi x}{2L} \sin\frac{j\pi x}{2L} dx \tag{B60}$$

$$IN54 = \int_{L_1}^{L} h_T h^{L} \sin\frac{i\pi x}{2L} \sin\frac{j\pi x}{2L} dx \tag{B61}$$

$$IN55 = \int_{L_1}^{L} h_T \cos\frac{i\pi x}{L} \sin\frac{j\pi x}{2L} dx \tag{B62}$$

where h_T is the thickness of the plate within the joint.

VITA

Jack E. Helms, Jr. was born in Hot Springs, Arkansas, in 1948. He received a bachelor of science degree in Mathematics in 1970 from Henderson State College. Jack served as an U.S. Army Engineer Officer in the Viet Nam War. Jack was elected into Pi Tau Sigma National Mechancial Engineering Honor Fraternity in 1973. He received a bachelor of science degree in Mechanical Engineering in 1974 and a master of science degree in Mechanical Engineering in 1975, both from the University of Arkansas. His master's thesis was awarded First Prize in the Graduate Manufactured Products Division of the Lincoln Arc Welding Contest in 1974. He is a member of the American Society of Mechanical Engineers and the American Welding Society. He has 24 years of engineering experience, most of which has been in the Chemical Process Industry. For the past six years Jack has served on Subcommittee 1 of the Association of American Railroads Tank Car Committee and the Rail Equipment Work Group of the Chemical Manufacturers Association. He has published nine technical papers during his time at L.S.U. He is a candidate for the degree of Doctor of Philosophy, which will be awarded in May, 1998.

DOCTORAL EXAMINATION AND DISSERTATION REPORT

Candidate: Jack E. Helms, Jr.

Major Field: Mechanical Engineering

Title of Dissertation: ANALYSIS OF TAPER-TAPER ADHESIVE-BONDED JOINTS IN COMPOSITE PLATES UNDER TENSION AND CYLINDRICAL BENDING

Approved:

Su-Seng Pang
Major Professor and Chairman

Dean of the Graduate School

EXAMINING COMMITTEE:

George E. Knight

John R. Collier

William A. Cabins

Chilan Yang (Co-Chair)

Date of Examination:

March 17, 1998

IMAGE EVALUATION TEST TARGET (QA-3)

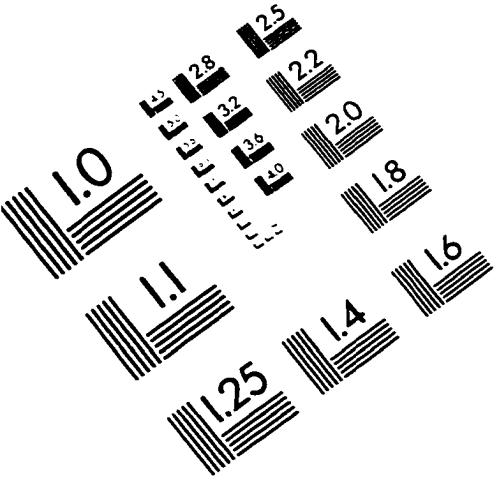

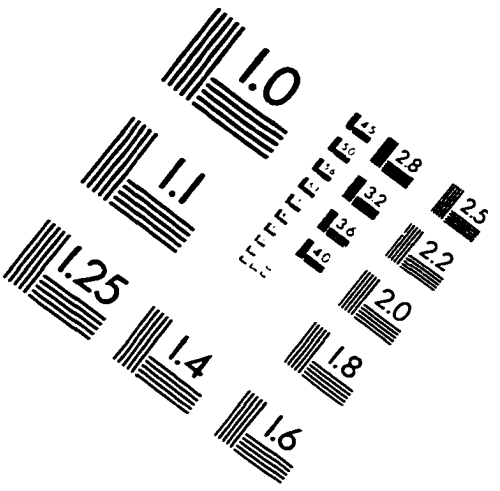

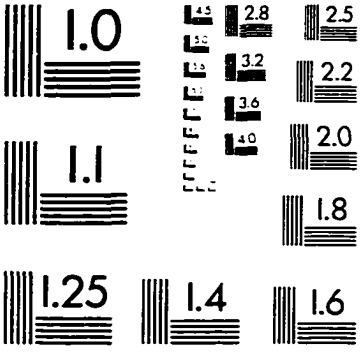

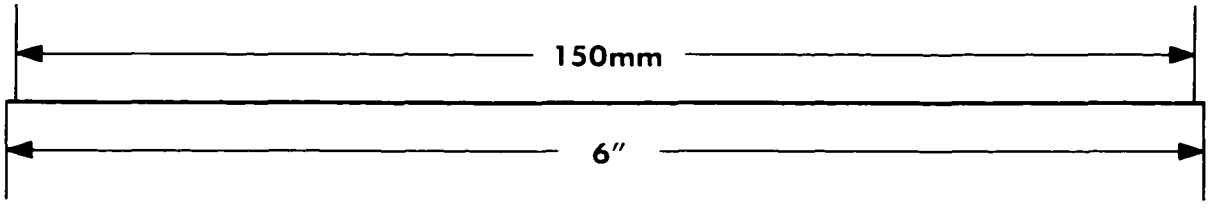

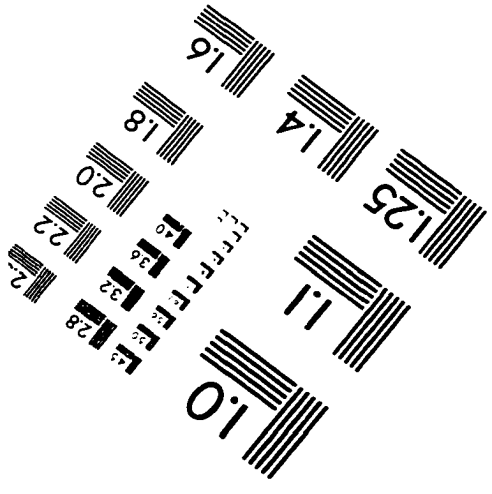

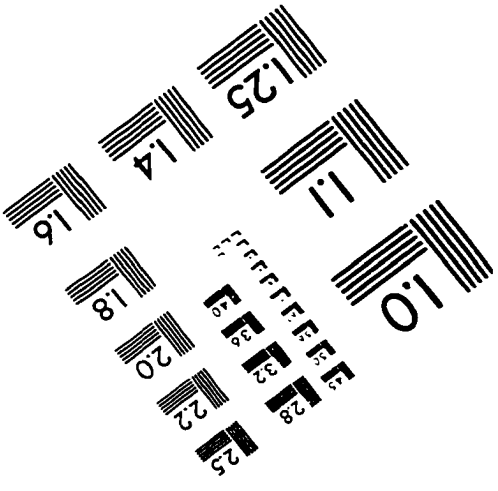

APPLIED IMAGE, Inc
1653 East Main Street
Rochester, NY 14609 USA
Phone: 716/482-0300
Fax: 716/288-5989